



# Atmospheric CO<sub>2</sub>, CH<sub>4</sub>, and CO with the CRDS technique at the Izaña Global GAW station: instrumental tests, developments, and first measurement results

Angel J. Gomez-Pelaez<sup>1,a</sup>, Ramon Ramos<sup>1</sup>, Emilio Cuevas<sup>1</sup>, Vanessa Gomez-Trueba<sup>1,2</sup>, and Enrique Reyes<sup>1</sup>

<sup>1</sup>Izaña Atmospheric Research Centre, Meteorological State Agency of Spain (AEMET), Tenerife, Spain

<sup>2</sup>Air Liquide España, Delegación Canarias, Tenerife, Spain

<sup>a</sup>now at: Meteorological State Agency of Spain (AEMET), Delegation in Asturias, Oviedo, Spain

**Correspondence:** Angel J. Gomez-Pelaez (agomezp@aemet.es)

Received: 14 October 2017 – Discussion started: 1 November 2017

Revised: 17 February 2019 – Accepted: 6 March 2019 – Published: 3 April 2019

**Abstract.** At the end of 2015, a CO<sub>2</sub>/CH<sub>4</sub>/CO cavity ring-down spectrometer (CRDS) was installed at the Izaña Global Atmosphere Watch (GAW) station (Tenerife, Spain) to improve the Izaña Greenhouse Gases GAW Measurement Programme, and to guarantee the renewal of the instrumentation and the long-term maintenance of this program. We present the results of the CRDS acceptance tests, the raw data processing scheme applied, and the response functions used. Also, the calibration results, the implemented water vapor correction, the target gas injection statistics, the ambient measurements performed from December 2015 to July 2017, and their comparison with other continuous in situ measurements are described. The agreement with other in situ continuous measurements is good most of the time for CO<sub>2</sub> and CH<sub>4</sub>, but for CO it is just outside the GAW 2 ppb objective. It seems the disagreement is not produced by significant drifts in the CRDS CO World Meteorological Organization (WMO) tertiary standards. The more relevant contributions of the present article are (1) determination of linear relationships between flow rate, CRDS inlet pressure, and CRDS outlet valve aperture; (2) determination of a slight CO<sub>2</sub> correction that takes into account changes in the inlet pressure/flow rate (as well as its stability over the years), and attributing it to the existence of a small spatial inhomogeneity in the pressure field inside the CRDS cavity due to the gas dynamics; (3) drift rate determination for the pressure and temperature sensors located inside the CRDS cavity from the CO<sub>2</sub> and CH<sub>4</sub> response function drift trends; (4) the determination of the H<sub>2</sub>O correction for CO has been performed using raw spectral peak data instead of the raw CO provided by

the CRDS and using a running mean to smooth random noise in a long water-droplet test (12 h) before performing the least square fit; and (5) the existence of a small H<sub>2</sub>O dependence in the CRDS flow and of a small spatial inhomogeneity in the temperature field inside the CRDS cavity are pointed out and their origin discussed.

## 1 Introduction

A CO<sub>2</sub>/CH<sub>4</sub>/CO cavity ring-down spectrometer (CRDS) was installed at the Izaña Global Atmosphere Watch (GAW) station (Tenerife, Spain) at the end of 2015 in order to improve the Izaña Greenhouse Gas (GHG) GAW Measurement Programme, and to guarantee the long-term maintenance of this program. The incorporation of the CRDS technique for the measurement of atmospheric CO<sub>2</sub>, CH<sub>4</sub>, and CO mole fractions was a recommendation of the World Meteorological Organization (WMO) World Calibration Centre (WCC) EMPA after its audit carried out at the Izaña Observatory (IZO) in September 2013 (EMPA, 2013).

The WMO GAW program requires high precision and accuracy in atmospheric GHG measurements, which are more stringent for trace gases with a longer lifetime in the atmosphere. The reason is that atmospheric GHG spatial gradients contain useful information about the spatial distribution of the surface sources and sinks of these trace gases (Chevallier et al., 2010), but these gradients decrease in absolute value as the trace gas lifetime increases (Patra et al., 2014). The GAW

required compatibility between laboratories is 0.1 ppm (parts per million in dry mole fraction; i.e., micromoles per mole of dry air) for carbon dioxide in the Northern Hemisphere and 0.05 ppm in the Southern Hemisphere; for methane, 2 ppb (parts per billion in dry mole fraction; i.e., nanomoles per mole of dry air); and for carbon monoxide, 2 ppb (WMO, 2016).

The CRDS technique (Crosson, 2008) has improved considerably the stability and precision in the raw measurements compared to those of older techniques (e.g., non-dispersive infrared analyzers, NDIRs, gas chromatography, GC, with a flame ionization detector, FID, and GC with a reduction gas detector, RGD); therefore, the required frequency of use of calibrating/reference gases to achieve the GAW data quality objectives (DQOs) is much lower. Additionally, this spectrometric technique does not require chromatographic gases (e.g., carrier gas, makeup gas, and FID gases for maintaining the flame), which are expensive and require great logistics efforts at remote stations. Zellweger et al. (2016) found out, when evaluating the results of scientific audits performed at GAW stations, that the results using newer spectroscopic techniques (CRDS and off-axis integrated cavity output spectrometry, OAICOS), in general, are better than those obtained with older techniques.

The Izaña Observatory is a Global GAW station located at 2373 m a.s.l. on Tenerife (Canary Islands, Spain), usually above a strong subtropical temperature inversion. Since it is located at the summit of a mountain, during nighttime there are North Atlantic free-troposphere background conditions, whereas during daytime there is a slight perturbation of these conditions by the arrival of an upslope thermal wind close to the terrain surface (e.g., Cuevas et al., 2013; Gomez-Pelaez et al., 2013; Rodríguez et al., 2009). Detailed information about the numerous measurement programs in operation at IZO is provided by Cuevas et al. (2015).

This paper presents the implementation of a CRDS G2401 at IZO and the development of the raw data processing scheme. The more relevant contributions of the present article are (1) determining linear relationships between flow rate, CRDS inlet pressure, and CRDS outlet valve aperture; (2) determining a slight CO<sub>2</sub> correction that takes into account changes in the inlet pressure/flow rate (as well as its stability over the years), and attributing it to the existence of a small spatial inhomogeneity in the pressure field inside the CRDS cavity due to the gas dynamics; (3) providing equations to determine the drift rate of the pressure and temperature sensors located inside the CRDS cavity from the CO<sub>2</sub> and CH<sub>4</sub> response function drift trends; (4) the determination of the H<sub>2</sub>O correction for CO has been performed using raw spectral peak data instead of the raw CO provided by the CRDS and using a running mean to smooth random noise in a long water-droplet test (12 h) before performing the least square fit; and (5) the existence of a small H<sub>2</sub>O dependence in the CRDS flow and of a small spatial inhomogeneity in the

temperature field inside the CRDS cavity are pointed out and their origin discussed.

The structure of this article is as follows. We firstly detail (Sect. 2) the results obtained in the initial tests performed on the Izaña CRDS (such as precision, repeatability, sensitivity to inlet gas pressure and response function) as well as the relationships between flow rate, CRDS inlet pressure, and CRDS outlet valve aperture; and the pre-processing applied to the raw data (Sect. 3). Secondly, we analyze the results of the calibrations performed every 3–4 weeks since the end of 2015 using WMO tertiary standards, and provide some details on the response functions used and the numerical processing software developed to evaluate the calibrations (Sect. 4). Thirdly, some details of the obtained and implemented water vapor corrections are provided (Sect. 5). Finally, the ambient measurements carried out until July 2017 are presented, as well as some details in the numerical processing software developed to obtain the ambient air CRDS measurements from raw data and calibration results, and compared with those obtained with other Izaña in situ measurement instruments (Sect. 6). In Sect. 7, a preliminary independent assessment on the drift rates of the CRDS CO standards is performed. The main conclusions are outlined in Sect. 8. A note concerning the inlet pressure (Sect. 2.4) and H<sub>2</sub>O dependences of the CRDS flow and the spatial inhomogeneity of the pressure field inside the CRDS cavity is presented (Appendix A). Additionally, we very briefly describe in Appendix C a few more novelties in the Izaña GHG Measurement Programme since the WMO/IAEA Meeting on Carbon Dioxide, Other Greenhouse Gases and Related Tracers Measurement Techniques that took place in the year 2015 (GGMT-2015).

## 2 Acceptance tests performed on the CRDS

A Picarro G2401 CRDS analyzer (serial number CFKADS2196) for measuring CO<sub>2</sub>, CH<sub>4</sub>, CO, and H<sub>2</sub>O was installed in November 2015 at IZO. Several acceptance tests were performed on the CRDS at the station, roughly following the recommendations provided by the European Integrated Carbon Observation System (ICOS)-Atmospheric Thematic Centre (ATC) (ICOS-ATC, 2016). To process the data associated with the tests, the raw values for CO<sub>2</sub> (not dry), CH<sub>4</sub> (not dry), CO, and H<sub>2</sub>O of the “Synchronized DataLog\_User” files were used.

### 2.1 Continuous measurement repeatability test

The first test was what ICOS-ATC (2016) called a “precision test”. This test is called continuous measurement repeatability (CMR) by Yver Kwok et al. (2015), and consists in measuring a gas cylinder (filled with dry natural air) over 25 h, rejecting the first hour as stabilization time. As Table 1 shows, the results (standard deviations) obtained in this test were

**Table 1.** Results obtained during the “precision test” (CMR) and ICOS-threshold values for two averaging times (1 and 60 min). The standard deviation (SD) reported is of the sample of 1 min (or 60 min) means obtained through the full duration of the test.

| Raw data<br>averagelength | CO <sub>2</sub> SD (ppm)<br>obtained/icos-threshold | CH <sub>4</sub> SD (ppb)<br>obtained/icos-threshold | CO SD (ppb)<br>obtained/icos-threshold | Mean H <sub>2</sub> O<br>(ppm) |
|---------------------------|---|---|--|--------------------------------|
| 1 min                     | 0.013/0.050   | 0.19/1.0  | 0.87/2.0                               | −2.8                           |
| 60 min                    | 0.009/0.025   | 0.14/0.5  | 0.16/1.0                               | −2.8                           |

**Table 2.** Results obtained during the “repeatability test” (LTR) and ICOS-threshold values. The SD reported is of the sample of 10 min means obtained through the full duration of the test.

| Cylinder | Average period<br>(10 min) | CO <sub>2</sub> SD (ppm)<br>obtained/icos-threshold | CH <sub>4</sub> SD (ppb)<br>obtained/icos-threshold | CO SD (ppb)<br>obtained/icos-threshold | Mean H <sub>2</sub> O<br>(ppm) |
|----------|----------------------------|---|---|--|--------------------------------|
| 1        | 20–30 min                  | 0.016/0.050   | 0.23/0.5  | 0.23/1.0                               | −1.3                           |
| 1        | 30–40 min                  | 0.021/–   | 0.34/–  | 0.28/–                                 | −1.8                           |
| 2        | 20–30 min                  | 0.016/0.050   | 0.23/0.5  | 0.35/1.0                               | −1.2                           |
| 2        | 30–40 min                  | 0.026/–   | 0.31/–  | 0.31/–                                 | −1.4                           |

well within the threshold established by ICOS-ATC (2016). Note that the precision for the H<sub>2</sub>O measurements indicated by the manufacturer of the CRDS is < 200 ppm for 5 s averages and < 50 ppm for 5 min averages. Therefore, it is reasonable to obtain small (in absolute value) negative values (−2.8 ppm) for H<sub>2</sub>O when measuring dry air, since, taking into account the precision of the instrument, these values are completely compatible with 0.0 ppm.

## 2.2 Long-term repeatability test

The second test performed was a “repeatability test” (this test is called long-term repeatability, LTR, by Yver Kwok et al., 2015). According to ICOS-ATC (2016), it consists in measuring alternately a gas cylinder (filled with dry natural air) during 30 min and ambient air (not dried) during 270 min over 72 h. Statistics are based only on the last 10 min average data for each gas cylinder “injection”. Indeed, we used two cylinders, each one measured every 5 h, with the following measurement cycle: cylinder 1 during 40 min, wet ambient air during 20 min, cylinder 2 during 40 min, and wet ambient air during 200 min. Table 2 shows the results obtained for each tank and 10 min average period: 20–30 and 30–40 min. The results were well within the thresholds established by ICOS-ATC (2016). Note that the SDs reported in Table 2 (associated with 10 min means) are larger for CO<sub>2</sub> and CH<sub>4</sub> (but lower for CO) than the SDs in Table 1 associated with 1 min means. This means the decrease in the random noise due to the increase in the averaging time is countered by the increase in the SD due to the larger response drift in the longer test (this is not the case for CO).

## 2.3 Ambient pressure sensitivity test

The third test performed was an ambient pressure sensitivity test for the measurements carried out during the mentioned period of 72 h; i.e., inlet gauge pressure was kept constant but the lab pressure (ambient pressure) was allowed to vary naturally. No pressure chamber was used, similarly to Yver Kwok et al. (2015). Note that this CRDS is not meant for use on aircraft, where large ambient pressure changes might occur. This test provides an upper limit for the ambient pressure sensitivity, since there might be instrumental drift not attributable to atmospheric pressure changes. The results obtained were 0.04 ppb hPa<sup>−1</sup> for CO, 0.0038 ppm hPa<sup>−1</sup> for CO<sub>2</sub>, and 0.047 ppb hPa<sup>−1</sup> for CH<sub>4</sub>. These sensitivities are not significant. The main purpose of this test was to confirm the CRDS CO measurements were not affected by natural ambient pressure changes, as indeed Yver Kwok et al. (2015) found for several CRDS units.

## 2.4 Relationships between inlet pressure, flow rate, and outlet valve aperture: inlet pressure sensitivity test

Due to their importance for the present article, we detail firstly the relationships we have found between inlet pressure, flow rate, and outlet valve opening.

According to the information provided by the manufacturer (Chris Rella, private communication, 2018), there is both a proportional valve and a physical critical orifice in the inlet system of the G2401 CRDS cavity. The proportional valve is opened slowly at start-up to ensure that the flow changes smoothly, but after this start-up procedure, the valve is set to open fully, and the flow is set by the critical orifice. There is also a proportional valve at the outlet of the cavity and upstream of the vacuum pump. The cavity (abso-

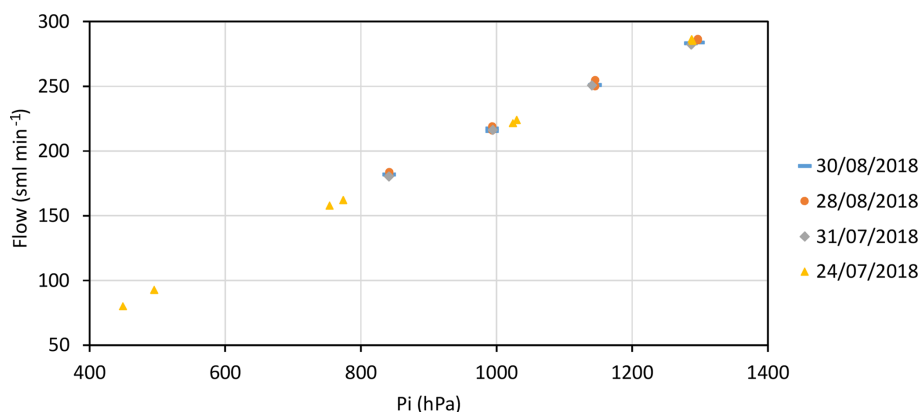


**Figure 1.** Results of tests performed on 4 non-consecutive days in which dry natural air coming from a standard was measured during many consecutive hours changing the CRDS inlet pressure every hour or longer.  $p_i$  is the CRDS inlet pressure and “Flow” is the flow measured downstream of the CRDS.

lute) pressure is kept at 186.7 hPa (140 Torr) by controlling the opening of the outlet valve (OV).

A choked flow is a flow through a critical orifice in which the following condition holds for the inlet to outlet (absolute) pressure ratio (Van den Bosch and Duijm, 2005):

$$\frac{p_i}{p_o} \geq \left( \frac{\gamma + 1}{2} \right)^{\gamma/(\gamma-1)}, \quad (1)$$

where  $p_i$  is the inlet (absolute) pressure,  $p_o$  is the outlet (absolute) pressure, and  $\gamma$  is the ratio of specific heats ( $c_p/c_v$ ) for the considered gas. For dry air,  $\gamma$  is equal to 1.4 and the right-hand side of Eq. (1) is equal to 1.893. In a choked flow, the speed is supersonic just downstream of the orifice and the flow rate does not depend on the downstream quantities (because “information” cannot propagate faster than sound). Since the minimal recommended inlet (absolute) pressure for the CRDS G2401 is 400 hPa, and the cavity pressure is 187 hPa (140 Torr), the flow in the inlet critical orifice is always choked. This is the reason why the flow through the CRDS cavity depends only on upstream quantities (mainly the inlet pressure) and not on the cavity quantities. However, for flight-ready models, the critical orifice is located at the outlet of the CRDS cavity, and therefore, the inlet pressure for the orifice is the cavity pressure, which is kept constant.

The theoretical equation relating the standard volumetric flow ( $F$ ) to the inlet quantities for a choked flow is (Van den Bosch and Duijm, 2005)

$$F = C_d \cdot A \cdot p_i \cdot \frac{T_s}{p_s} \cdot \left[ \frac{\gamma \cdot R}{T_i} \cdot \left( \frac{2}{\gamma + 1} \right)^{(\gamma+1)/(\gamma-1)} \right]^{1/2}, \quad (2)$$

where  $T_s$  and  $p_s$  are the standard (absolute) temperature (273.15 K) and pressure (1013.25 hPa), respectively,  $T_i$  is the inlet (absolute) temperature,  $R$  is the gas constant,  $C_d$  is the discharge coefficient (dimensionless) and  $A$  is the hole cross-sectional area. Equation (2) shows that the standard volumetric flow is proportional to the inlet (absolute) pressure and

inversely proportional to the square root of the inlet (absolute) temperature.

As indicated in Sect. 6, the ambient air/gas standard plumbing configuration operational since 28 November 2016, includes a Red-Y mass flow meter (MFM) downstream of the CRDS, but upstream of the vacuum pump. There is an expansion volume between the MFM and the vacuum pump to smooth the pulses induced in the flow by the pump.

The fourth acceptance test was an inlet pressure sensitivity test when measuring a gas cylinder filled with dry natural air. This test was performed on 25 and 26 November 2015. Additional more complete tests of that type were performed in July and August 2018.

Figure 1 shows results of that second set of tests (no flow rate measurements were carried out during the first set of tests) performed on 4 non-consecutive days in which dry natural air coming from a standard was measured during many consecutive hours changing the CRDS inlet pressure every hour or longer, discarding the first 20 min after the pressure change, and keeping the mean of the measurements till the next pressure change. The sequences of pressures used were not monotonic but with jumps up and down. Pressure was measured using the regulator gauge and then ambient pressure was summed. On 24 July 2018 the test was performed using a cylinder regulator of a different type than the one used the other 3 days. As Fig. 1 shows, the relationship between the CRDS inlet pressure and the flow rate is linear. Table 3 shows the coefficients and  $R^2$  obtained fitting a straight line to the data of each test. The linear fits are very good ( $R^2$  is almost 1) and very similar (the first one is slightly different, probably due to the use of a different regulator and a larger pressure range).

Figure 2 shows results of the first and second sets of inlet pressure sensitivity tests. The first tests were performed alternating only between two inlet pressures, using cylinder regulators different from those used in the second set of tests.

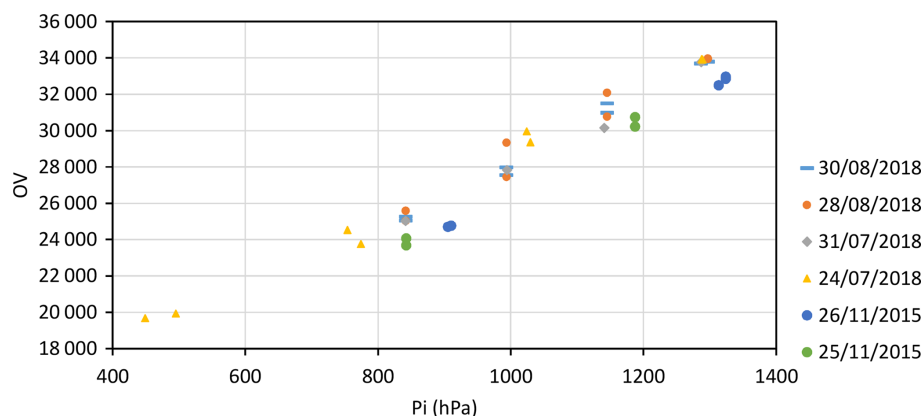


**Figure 2.** Results of the first and second sets of inlet pressure sensitivity tests.  $p_i$  is the CRDS inlet pressure and OV is the aperture of the CRDS-cavity outlet valve.

**Table 3.** Coefficients and  $R^2$  obtained fitting a straight line to the test data shown in Fig. 1. “sml” denotes standard milliliters.

| Test           | Slope<br>(sml (min hPa) <sup>-1</sup> ) | Intercept<br>(sml min <sup>-1</sup> ) | $R^2$  |
|----------------|---|---------------------------------------|--------|
| 24 July 2018   | 0.244                                   | -27.9                                 | 0.9998 |
| 31 July 2018   | 0.229                                   | -12.2                                 | 0.9996 |
| 28 August 2018 | 0.228                                   | -9.5                                  | 0.9984 |
| 30 August 2018 | 0.226                                   | -8.4                                  | 0.9996 |

**Table 4.** Coefficients and  $R^2$  obtained fitting a straight line to the test data shown in Fig. 2.

| Test             | Slope (hPa <sup>-1</sup> ) | Intercept | $R^2$  |
|------------------|----------------------------|-----------|--------|
| 25 November 2015 | 19.2                       | 7720      | 0.9954 |
| 26 November 2015 | 19.5                       | 7020      | 0.9996 |
| 24 July 2018     | 17.6                       | 11 300    | 0.9913 |
| 31 July 2018     | 19.2                       | 8710      | 0.9913 |
| 28 August 2018   | 19.1                       | 9320      | 0.9659 |
| 30 August 2018   | 19.5                       | 8660      | 0.9934 |

As Fig. 2 shows, the relationship between the CRDS inlet pressure and OV is linear. Table 4 shows the coefficients and  $R^2$  obtained fitting a straight line to the data of each test. The linear fits are very good ( $R^2$  is very near 1) and have very similar slopes (except for the test performed using a larger pressure range).

Figure 3 shows results of the inlet pressure sensitivity tests for CO<sub>2</sub>, CH<sub>4</sub> and CO, using OV as independent variable. Since the cylinders used were not unique, for each test we use the difference with respect to the mean raw mole fraction measured during the whole test and the symbol “d” to indicate such difference. As Fig. 3 shows, the relationship between  $dCO_{2raw}$  and OV is linear. Note that the  $dCO_{2raw}$  values are quite small, and therefore it is not surprising there is some noise in the fit, but the slopes obtained in the six tests are consistent. For  $dCH_{4raw}$  there is a linear relationship too, but noisier. For  $dCO_{raw}$  there is no significant linear relationship. Table 5 shows the mean slope and intercept for each trace gas as well as the associated standard deviations. Those numbers confirm the previous sentences concerning the statistical significance of the linear fits for CO<sub>2</sub>, CH<sub>4</sub> and CO.

Taking into account the linear relationship between inlet pressure and OV, and the values shown in Table 5, the sensitivities obtained were  $0.00 \times 10^{-2}$  ppb kPa<sup>-1</sup> (since the slope is not statistically significant) for CO,  $-0.83 \times$

$10^{-3}$  ppm kPa<sup>-1</sup> for CO<sub>2</sub>, and  $-0.47 \times 10^{-2}$  ppb kPa<sup>-1</sup> for CH<sub>4</sub>, which are quite small except for CO<sub>2</sub> (e.g., 30 kPa produces a bias of  $-0.025$  ppm in CO<sub>2</sub>). Since the CRDS inlet pressure can be different (e.g., differences of a few tens of kPa may be present) when changing the sample (laboratory standards, target gases and ambient air), and in order to be able to achieve a very accurate response function for CO<sub>2</sub>, we empirically correct for this effect as explained in Sect. 3.1.

## 2.5 Calibration curve fitting test

The fifth test was fitting response curves when calibrating with four WMO tertiary standards (six cycles, 2.5 h cycle<sup>-1</sup>; each standard is measured during 30 consecutive minutes as well as a target gas). When performing a linear fitting for CH<sub>4</sub>, the root mean square (rms, accounting for the effective degrees of freedom) residual was 0.143 ppb (very small). When performing a linear fitting for CO, the rms residual was 0.067 ppb (very small). However, when performing a linear fitting for CO<sub>2</sub>, the rms residual was 0.0395 ppb, which is larger than the values we usually obtain with our NDIR-based measurement system for CO<sub>2</sub> when using a quadratic fitting (Gomez-Pelaez and Ramos, 2011). Moreover, when using a quadratic fitting for the CRDS CO<sub>2</sub>, the rms residual was 0.0284 ppm, still slightly worse than that of our NDIR-

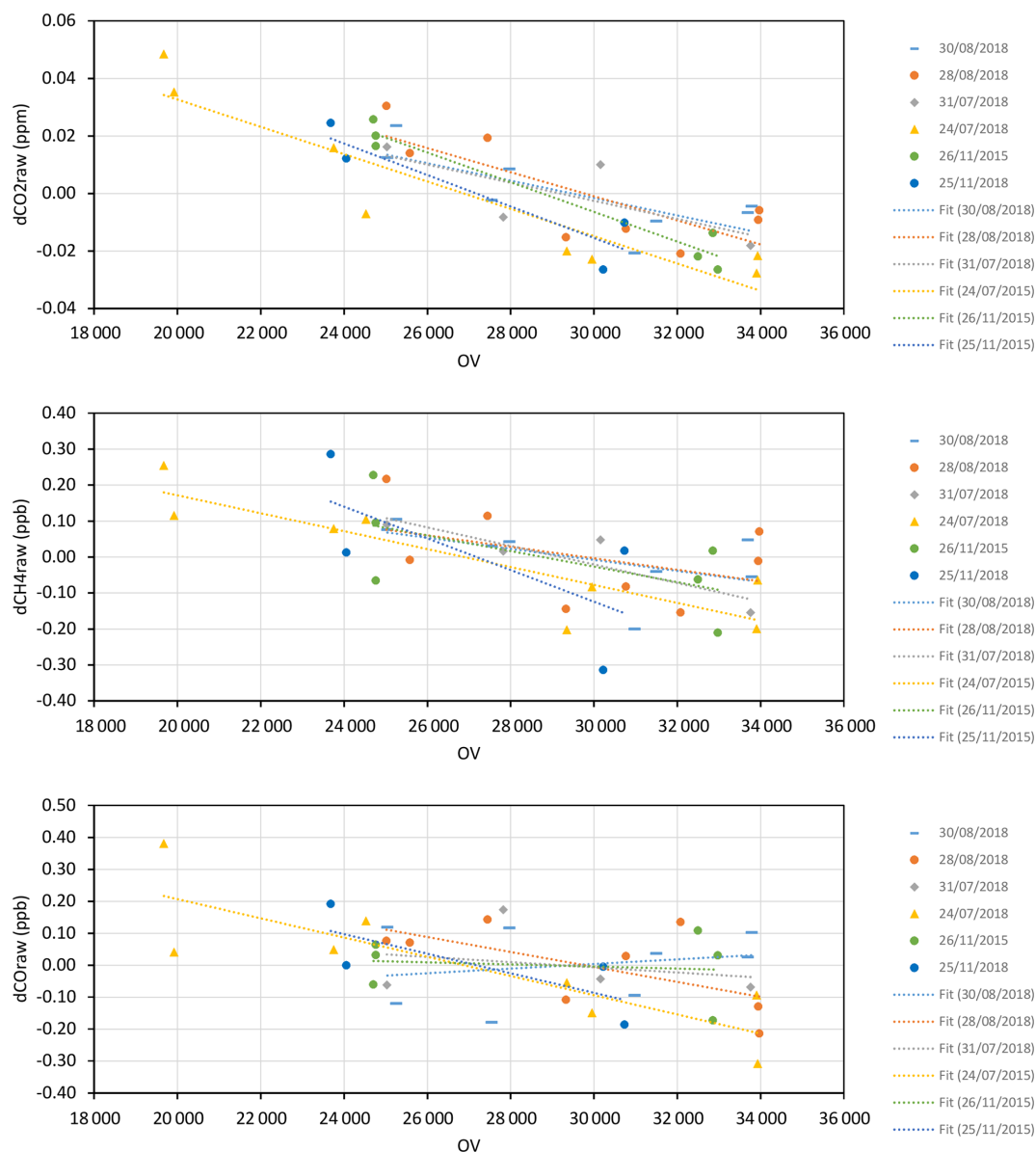


**Figure 3.** Results of the inlet pressure sensitivity tests for CO<sub>2</sub>, CH<sub>4</sub> and CO, using OV as an independent variable. For each test, “d” denotes the difference with respect to the mean raw mole fraction measured during the whole test.

**Table 5.** Mean slope and intercept for the fits (Fig. 3) associated with each trace gas (as well as the associated standard deviations, SDs) in the inlet pressure sensitivity tests.

| Trace gas       | Mean slope                 | SD                        | Mean intercept | SD        |
|-----------------|----------------------------|---------------------------|----------------|-----------|
| CO <sub>2</sub> | $-4.29 \times 10^{-6}$ ppm | $1.03 \times 10^{-6}$ ppm | 0.122 ppm      | 0.026 ppm |
| CH <sub>4</sub> | $-2.46 \times 10^{-5}$ ppb | $1.05 \times 10^{-5}$ ppb | 0.695 ppb      | 0.271 ppb |
| CO              | $-1.47 \times 10^{-5}$ ppb | $1.56 \times 10^{-5}$ ppb | 0.409 ppb      | 0.433 ppb |

based systems. Finally, when correcting the raw CO<sub>2</sub> from the inlet pressure sensitivity and then performing a quadratic fitting, the rms residual was 0.0219 ppm, which is similar to the values obtained with our NDIR-based systems. Dur-

ing the calibration described above, the inlet pressure differences were especially intense. We have improved our skills since then, getting smaller inlet pressure differences during the calibrations.

### 3 Data acquisition and pre-processing

Pre-processing refers to the computation of raw-data 30 s means and corresponding standard deviations using the *DataLog\_User* files (not the synchronized ones), as well as the computation of some derived variables detailed below. We have developed the pre-processing software, as well as the calibration and ambient-air processing software. For the computation of 30 s means and standard deviations, we take into account the so-called “species” field. The species code is different for each spectral range in which the measurements are performed. There are four spectral ranges and three lasers, since two nearby spectral ranges are scanned with the same laser (see Chen et al., 2010, 2013, for details about these spectral ranges). The fields updated in each file line are those related to the spectral lines measured in the corresponding spectral range. The *DataLog\_User* file contains 1.7 lines/s, and these lines follow this time sequence of species: 1, 2, 4, and 3. The raw variables associated with each “species” value are (a) Species = 1, CO<sub>2</sub>, *peak\_14* (*p14*), and CO; (b) Species = 2, CH<sub>4</sub>, *CO2\_dry*; (c) Species = 3, H<sub>2</sub>O, *h2o\_reported* (*hr*), *CO2\_dry*, and *CH4\_dry*; and (d) Species = 4, CO, *b\_h2o\_pct* (*bh*), and *peak84\_raw* (*p84*); where CO<sub>2</sub> and CH<sub>4</sub> are raw values not corrected from H<sub>2</sub>O dilution nor pressure broadening, whereas *CO2\_dry* and *CH4\_dry* have been (factory) corrected from those effects, *p14* is the raw value associated with the main CO<sub>2</sub> peak, CO is already (factory) corrected from the CO<sub>2</sub> and H<sub>2</sub>O influences, H<sub>2</sub>O is the calibrated value obtained from *hr*, which is the reported H<sub>2</sub>O raw value associated with the main H<sub>2</sub>O peak (in the CH<sub>4</sub>-peak laser wavelength range), *bh* is the H<sub>2</sub>O raw value associated with the secondary H<sub>2</sub>O peak (in the CO-peak laser wavelength range), and *p84* is the raw value associated with the CO peak. Additionally, there are other raw variables not associated with a single “species” value that we use: cavity pressure (CP), cavity temperature (CT), multi-position valve (MPV) position (MPVP), outlet valve (OV), and solenoid valves (SVs). Note that the Picarro software is able to control both solenoid (up to six) and MPV (just one) valves for the gas handling system, and stores the positions of the valves in the same file as the output data for the measured trace gases. The information on the positions of the solenoid valves is codified in a single natural number (SV).

A 30 s mean is accepted when (a) at least 85 % of the expected data are present and (b) all the instantaneous data have the same MPVP and SV values. Additionally, a counter called “npcmc” is assigned to each 30 s mean. It indicates the number of consecutive 30 s means with the same configuration for both MPVP and SV.

#### 3.1 Inlet pressure sensitivity correction for raw CO<sub>2</sub>

We use the original empirical relationship we determined through the inlet pressure sensitivity test mentioned in

Sect. 2.4, which leads to the following outlet-valve-corrected raw CO<sub>2</sub>:

$$CO2_{ovc} = CO2_{raw} + 0.04 \cdot (OV - 26468.15)/7700. \quad (3)$$

*CO2<sub>ovc</sub>* is the raw value we use for the CO<sub>2</sub> processing. These slope and intercept values are compatible with the corresponding mean values shown in Table 5 (distant less than 1 standard deviation from the corresponding mean). *CO2<sub>ovc</sub>* is corrected from the inlet pressure sensitivity but not for the H<sub>2</sub>O dilution and pressure broadening. According to the knowledge of the authors, this is a new correction not considered previously in the scientific literature.

Note that if Eq. (3) is expanded, only the slope term in OV is kept fixed, since the independent term is, in practice, combined with the independent term of the mole-fraction calibration curve (see Sect. 4), which is updated periodically. Therefore, this automatically takes into account hypothetical drifts in the independent term of Eq. (3). As Fig. 2 and Table 4 show, the slope of the linear relationship between OV and *p<sub>i</sub>* is consistent through the years, and no significant change in time is observed in the slope of the linear relationship between *dCO2<sub>raw</sub>* and OV. Note that if we average the addends of Eq. (3) and subtract those from Eq. (3), we obtain an equation for *dCO2<sub>raw</sub>* that is linear in OV and has an intercept that depends on the average OV. This explains why in Fig. 3a, the fit for the test with the largest OV range (smallest average OV) is below the rest of the test fits.

In Appendix A, we provide a plausible physical explanation for this effect, after determining the H<sub>2</sub>O dependence of the CRDS flow and arguing that the pressure field inside the CRDS cavity is slightly inhomogeneous. Note that our arguments that point out to the fact that the inhomogeneity of the pressure field inside the cavity due to the flow produces the CO<sub>2<sub>raw</sub></sub> dependence on the OV, seem also to be supported by the following fact: the relative effect of the flow on CO<sub>2<sub>raw</sub></sub> and CH<sub>4<sub>raw</sub></sub> is roughly the same, as we could roughly expect from the decrease in trace gas concentration (mol per volume) that takes place inside the CRDS cavity near the inlet and outlet, due to the decreased pressure (see Appendix A). Note that, dividing the slopes of Table 5 by the typical ambient air mole fraction at IZO (405 ppm for CO<sub>2</sub> and 1880 ppb for CH<sub>4</sub>), we obtain  $1.06 \times 10^{-8}$  for CO<sub>2</sub> and  $1.31 \times 10^{-8}$  for CH<sub>4</sub>.

#### 3.2 Raw CH<sub>4</sub>

We call CH<sub>4<sub>raw</sub></sub> the raw CH<sub>4</sub> multiplied by 1000 (to have ppb units) and use it for the CH<sub>4</sub> processing. Note that CH<sub>4<sub>raw</sub></sub> is the wet value not corrected from H<sub>2</sub>O dilution and pressure broadening.

#### 3.3 Computed raw wet CO

The CO value provided by the G2401 CRDS includes the correction due to H<sub>2</sub>O dilution and pressure broadening.

However, what we use for CO processing is the CO raw value (wet) that Picarro calls *peak84\_spec\_wet* (*p84sw*), which is *p84* corrected from the H<sub>2</sub>O and CO<sub>2</sub> spectral peak overlapping (interference that changes the zero of *p84*). To compute it, we use the equations that our G2401 employs internally (Chris Rella, private communication, 2016):

$$co2\_p14 = 0.706630873 \cdot p14, \quad (4)$$

$$p84sw = p84 + off + w1 \cdot bh + wc \cdot bh \cdot co2\_p14 + w2 \cdot bh^2 + c1 \cdot co2\_p14, \quad (5)$$

where  $off = -0.000800885106752$ ,  $w1 = -0.0334069906515$ ,  $wc = -8.2480775807 \times 10^{-7}$ ,  $w2 = 0.00633381386844$ , and  $c1 = 8.87510231866 \times 10^{-6}$ . We denote *p84sw'*, *p84sw* multiplied by 1000. That is the raw value we use for the CO processing; i.e., it is the wet value not corrected from H<sub>2</sub>O dilution and pressure broadening nor converted to ppb units.

#### 4 Calibrations and response functions

After processing, the measurements we carry out with the CRDS are in the following WMO scales: X2007 for CO<sub>2</sub>, X2004A for CH<sub>4</sub> and X2014A for CO, since we use four multi-species WMO tertiary standards filled (with dried natural air) and calibrated by the WMO Central Calibration Laboratory (CCL) for these gases (<https://www.esrl.noaa.gov/gmd/ccl/>, last access: 26 March 2019).

In each cycle of a calibration we use the four WMO tertiary standards and two target gases that act as unknowns. Each tank is measured continuously during 30 min every cycle. From December 2015 to August 2016, each calibration had five cycles and a calibration was performed every 3 weeks. From September 2016 till present, each calibration has two cycles and a calibration is performed every month. In the first period, we adopted a conservative strategy, and after analyzing the obtained results in detail we concluded that the second calibration strategy provided results that satisfied our accuracy requirements. Note that since there are technicians at the station every day, the regulators of the WMO tertiary standards remain closed between calibrations. This helps avoid any hypothetical problem of drifting in the standards due to very small leaks or differential diffusion inside the regulators that might propagate to the interior of the cylinders through the open valves by diffusion during the weeks the standard air remains static inside the regulators. For CO<sub>2</sub> and CH<sub>4</sub>, the last 10 min of each gas injection are used. However, for CO, the last 20 min are used since CO measurements are noisier (i.e., better signal to noise ratio when incrementing the averaging period), and 10 min of stabilization time is enough for CO (numerical details not presented here).

The calibration processing is done using our own numerical code. To process a calibration, the code computes the

mean raw response for each tank and species, and then performs a least-square fit to the respective response function detailed below. For CH<sub>4</sub> and CO, we use linear response functions

$$CH4raw = b \cdot CH_4 + c, \quad (6)$$

and

$$p84sw' = b \cdot CO + c, \quad (7)$$

where CH<sub>4</sub> and CO are the dry mole fractions (the gas standards are dry) in ppb assigned by the CCL on the WMO scales. We have preferred to use a quadratic fit instead of a linear fit for CO<sub>2</sub>, since the rms residual is significantly smaller: considering the first 13 calibrations, the mean rms residual for linear fits is 0.035 ppm, whereas for quadratic fits it is 0.020 ppm. As mentioned in Sect. 2.5, we have chosen the quadratic fit for CO<sub>2</sub> to obtain rms residuals as small as we obtain with the IZO NDIR-based measurement system. The quadratic function with a raw signal slightly corrected in the outlet valve aperture used (as described in Sect. 3.1) is

$$CO2ovc = a \cdot CO_2^2 + b \cdot CO_2 + c, \quad (8)$$

where CO<sub>2</sub> is the dry mole fraction in ppm assigned by the CCL on the WMO scale. Since *b* is always positive (and near 1) and *a* is always negative and near zero, CO<sub>2</sub> is given by this solution of the second-order algebraic Eq. (8):

$$CO_2 = \left[ -b + \sqrt{b^2 - 4 \cdot a(c - CO2ovc)} \right] / (2 \cdot a). \quad (9)$$

To assess the drift in time of the response function from December 2015 to July 2017, we use the concept of virtual tank of fixed (assigned WMO; i.e., CO<sub>2</sub>, CH<sub>4</sub>, and CO) mole fractions (Yver Kwok et al., 2015) and compute the raw values (*CO2ovc*, *CH4raw*, and *p84sw'*) associated with those mole fractions using the response functions obtained in the calibrations. We consider a virtual tank with 400 ppm of CO<sub>2</sub>, 1850 ppb of CH<sub>4</sub> and 100 ppb of CO. Moreover, we present here a justification of that procedure and complement it by using the local slope of the response function at the mole fraction of the virtual tank for each species. In the field of high-accuracy atmospheric trace-gas measurements, the calibration fits are generally performed using a limited range in the independent variable that is far from zero (a range around the atmospheric mole fractions of interest). This produces an anticorrelation between the coefficients *b* and *c*. The reason is the fact that if *b* has a positive error (larger slope) then *c* will have a negative error (smaller *Y* intercept) that will increase in absolute value as the distance between the used *X* range and zero increases. Therefore, plotting the time series *b* and *c* is not the best option for assessing the stability in time of the response function, since part of the variability is due to the anticorrelation and does not correspond with a real

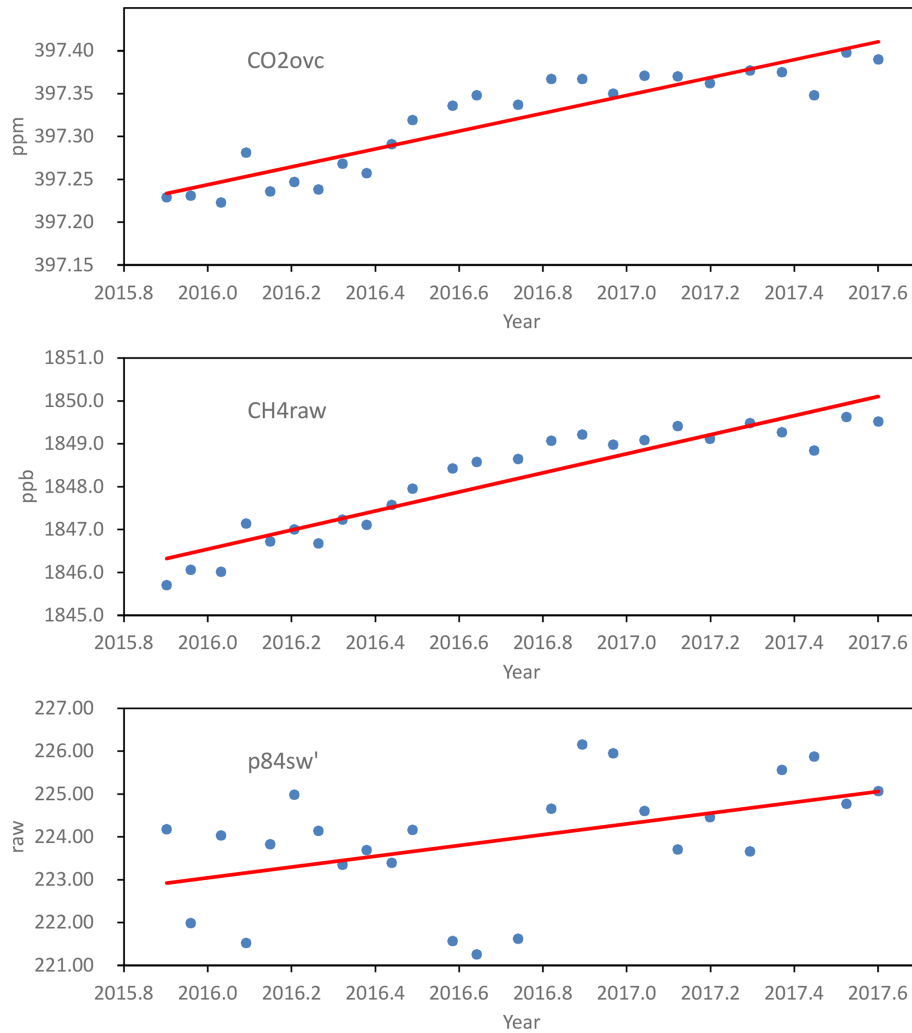


**Figure 4.** CRDS raw responses (blue dots) for a virtual tank (400 ppm of CO<sub>2</sub>, 1850 ppb of CH<sub>4</sub>, and 100 ppb of CO) computed using the response functions obtained in the calibrations. Each red line corresponds to a least-square fitting of the data to a linear function.

variability within the  $X$  range of interest. A more interesting option is to plot the  $Y$  value corresponding to a  $X$  value located within the range of interest instead of  $c$  (virtual tank concept) and the local slope at that  $X$  value. Note that for CH<sub>4</sub> and CO, which have linear response functions, the local slope does not depend on mole fraction and is equal to the coefficient  $b$ .

Figure 4 shows the CRDS raw responses for that virtual tank computed using the response functions obtained in the calibrations. From Fig. 4, we obtain the CRDS long-term drift of the raw responses: 0.104 ppm year<sup>-1</sup> for CO<sub>2</sub>, 2.22 ppb year<sup>-1</sup> for CH<sub>4</sub>, and 0.544 ppb year<sup>-1</sup> for CO.

As Yver Kwok et al. (2015), we define the fractional variables  $CH4frac = CH4raw / 1850$  and  $CO2frac = CO2ovc / 400$ , i.e., as the raw mole fractions of the virtual tank divided by the real mole fractions. Figure 5 shows a scatter plot of  $CH4raw$  vs.  $CO2ovc$  for the virtual tank. When fitting a linear function, the obtained

slope is 20.788 ppb ppm<sup>-1</sup>, which is equal to 4.495 when using the fractional variables,  $CH4frac$  and  $CO2frac$ .

Assuming that those drifts are due to drifts in the real pressure and temperature of the cavity (i.e., drifts in the  $P$  and  $T$  sensors that, in turn, cause the cavity to be controlled at slightly drifting pressure and/or temperature), taking into account the fact that the empirical sensitivities (partial derivatives) of the CRDS raw CO<sub>2</sub> and CH<sub>4</sub> with respect to CP and CT are known (Sect. 3.3.6 of Yver Kwok et al., 2015), and using these general relationships between partial derivatives:

$$\frac{dCH4frac}{dCO2frac} = \frac{\left(\frac{\partial CH4frac}{\partial T} \cdot \frac{dT}{dp} + \frac{\partial CH4frac}{\partial p}\right)}{\left(\frac{\partial CO2frac}{\partial T} \cdot \frac{dT}{dp} + \frac{\partial CO2frac}{\partial p}\right)}, \quad (10)$$

and

$$\frac{dCH4frac}{dt} = \left(\frac{\partial CH4frac}{\partial T} \cdot \frac{dT}{dp} + \frac{\partial CH4frac}{\partial p}\right) \frac{dp}{dt}. \quad (11)$$

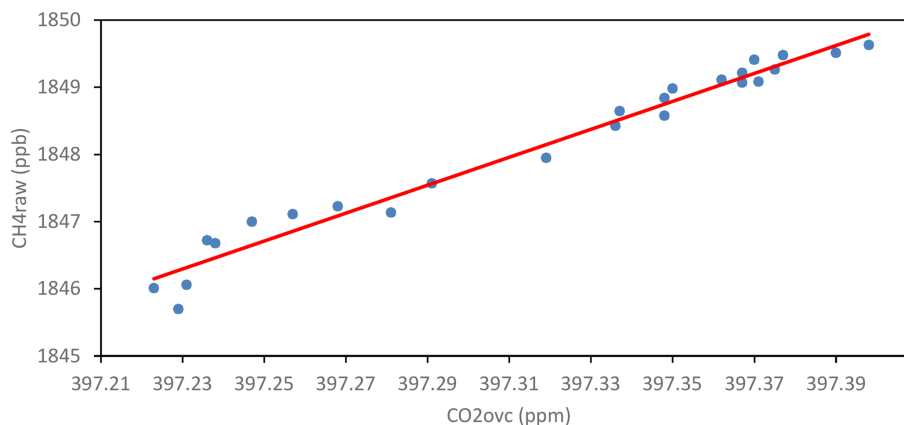


**Figure 5.** Scatter plot of  $CH_4raw$  vs.  $CO_2raw$  for the mentioned virtual tank. The red line has been obtained performing a least-square fitting of the data to a linear function.

We have determined that our CRDS has a long-term drift of  $0.114\text{ }^{\circ}\text{C hPa}^{-1}$  (obtained using Eq. 10 and taking into account that the left-hand side of Eq. 10 is equal to the slope shown in Fig. 5 multiplied by  $400/1850$ ),  $0.595\text{ hPa year}^{-1}$  (obtained using Eq. 11 and taking into account that the left-hand side of Eq. 11 is equal to the slope shown in Fig. 4b divided by 1850), and  $0.0678\text{ }^{\circ}\text{C year}^{-1}$  (obtained multiplying the two former numbers) in the cavity sensors. Note that the use of Eqs. (10) and (11), which provide a quantitative estimation of the drift in temperature and pressure, is new in the GHG monitoring literature. The fact that the drifts in temperature and pressure are linear in time is a consequence of the fact that the slopes shown in Figs. 5, 4a and b are constant, and from Eqs. (10) and (11).

Figure 6 provides additional information about the response functions determined in the calibration. In detail, Fig. 6 provides for each species the local slope of the response function at the mole fraction of the virtual tank, as well as the quadratic coefficient ( $a$ ) for the CO<sub>2</sub> response function.

Figure 7 provides for each species and calibration the rms residual of the fit and the difference between the assigned mole fraction to a target gas and the mean mole fraction of such target gas. For CO<sub>2</sub>, the mean rms residual for all the calibrations is 0.021 ppm, there is no trend in the associated time series, and the maximum departure in absolute value of a target gas assignment from the mean for such target gas is 0.026 ppm. Those numbers are quite small compared with the GAW DQO for CO<sub>2</sub>, and indicate a good performance of the measurement system for CO<sub>2</sub>. For CH<sub>4</sub>, the mean rms residual for all the calibrations is 0.09 ppb, there is no trend in the associated time series, and the maximum departure in absolute value of a target gas assignment from the mean for such target gas is 0.18 ppb. As for CO<sub>2</sub>, those numbers are quite small compared with the GAW DQO for CH<sub>4</sub> and indicate a good performance of the measurement system for CH<sub>4</sub>. However, for CO, there is a significant trend in the time series

of rms residuals, which show a value of around 0.1 ppb for the first calibrations, but increasing to around 0.7 ppb for the last calibrations. Moreover, there are significant downward drifts in all the time series of target gas assignments, which is a very strange fact since CO standards normally drift upward (i.e., when a CO standard drifts, this drift is generally positive; e.g., [https://www.esrl.noaa.gov/gmd/ccl/co\\_scale.html](https://www.esrl.noaa.gov/gmd/ccl/co_scale.html), last access: 26 March 2019). All these facts suggest that the IZO CRDS CO WMO tertiary standards might be drifting upward quite significantly at different rates. In Sect. 7, this possibility is investigated.

## 5 Water vapor correction: water-droplet method

The natural air contained in the WMO tertiary standards and the target standards is dry. However, ambient air contains water vapor and if it is not completely dried before measurements (as is done in NDIRs), the dilution and pressure broadening effects due to H<sub>2</sub>O need to be taken into account and corrected (Chen et al., 2010, 2013; Zellweger et al., 2012; Rella et al., 2013; Karion et al., 2013).

To determine the particular water vapor dilution and pressure broadening corrections for IZO CRDS G2041, we performed a long water-droplet test (around 12 h) using crushed (to increase the surface / volume ratio) silica gel balls soaked with deionized water contained in a stainless steel filter housing (called MPI/NOAA implementation in Rella et al., 2013), as Fig. 8 shows. The dry natural air coming from a standard flowed continuously around 12 h through the wet silica gel before being measured in the CRDS. Figure 9 shows the evolution in time of the  $h_2o\_reported$  ( $hr$ ) in pph (parts per hundred in mole fraction, i.e., centimoles per mole of air) determined by the CRDS.

For CO<sub>2</sub> and CH<sub>4</sub>, we use these empirical correction equations for the H<sub>2</sub>O dilution and pressure broadening effects (Chen et al., 2010):

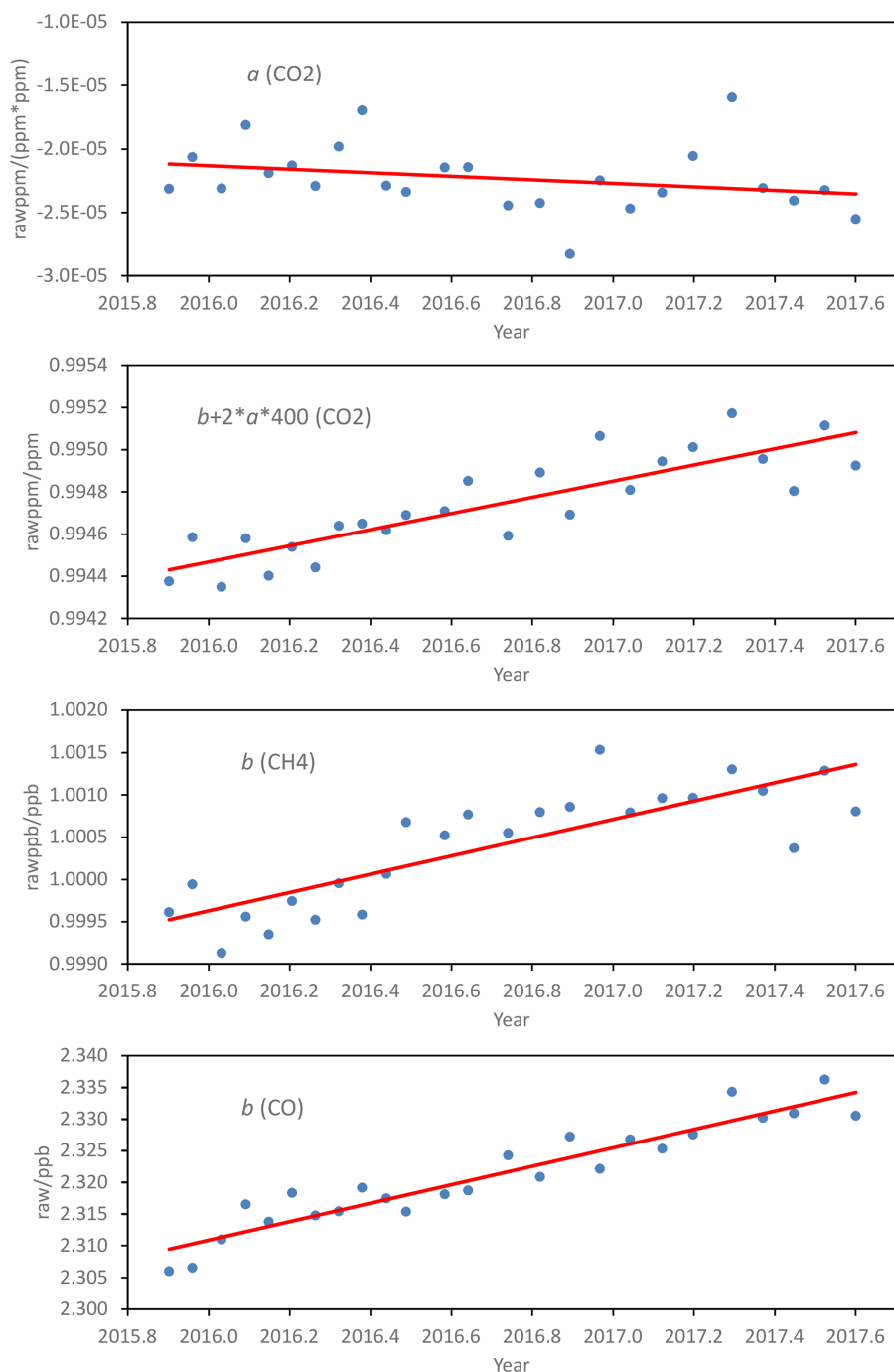


**Figure 6.** Quadratic coefficient of the CO<sub>2</sub> response function ( $a$ ) and local slope of the response function at the mole fraction of the virtual tank, for CO<sub>2</sub>, CH<sub>4</sub>, and CO. Note that for CH<sub>4</sub> and CO, the local slope does not depend on the mole fraction and is equal to the coefficient  $b$ . The red line corresponds to a least-square fitting of the data to a linear function.

$$CO2ovc_{wet} = CO2ovc_{dry} \cdot (1 + d \cdot hr + e \cdot hr^2), \quad (12)$$

$$CH4raw_{wet} = CH4raw_{dry} \cdot (1 + d \cdot hr + e \cdot hr^2), \quad (13)$$

where  $CO2ovc_{dry}$ ,  $CH4raw_{dry}$ ,  $d$ , and  $e$  (different in each equation) are determined by least-square fitting to test re-

sults. Since the experiment is very long, before performing the least-square fit, we aggregate data computing 100-data means. That corresponds approximately to a 59 s mean, since there are 1.7 data s<sup>-1</sup>. For CO<sub>2</sub>, we obtained coefficients  $d$  and  $e$  very close to those reported by Chen et al. (2010). Thus, we decided to use their coefficients,  $d = -0.012 \text{ pph}^{-1}$



**Figure 7.** The rms residual of the fit (red dots/line) and the difference between the assigned mole fraction to a target gas and the mean mole fraction of such a target gas (a different color is used for each target gas), for each species and mole-fraction calibration performed using four WMO laboratory standards (every 3 or 4 weeks).

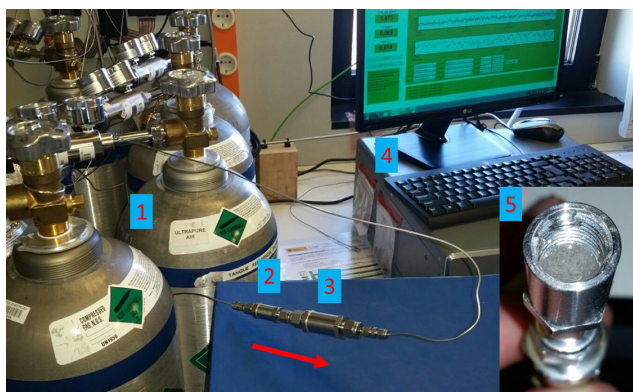


**Figure 8.** Experimental setup used for the water-droplet test performed on IZO CRDS G2401. (1) Cylinders containing dry natural air (the red arrow shows the flow direction); (2) stainless steel filter housing containing crushed silica gel balls (see details of the interior in 5) soaked with deionized water; (3) stainless steel 0.5  $\mu\text{m}$  filter; and (4) CRDS.

and  $e = -0.000267 \text{ pph}^{-2}$ . However, in Appendix B, we provide Fig. B1, which shows  $CO2_{ovc\_wet}$  vs.  $hr$  during the experiment, because it is going to be referenced in the present section when discussing a related topic. Figure 10 shows  $CH4_{raw\_wet}$  vs.  $hr$  during the experiment and the least-square fitted curve, the coefficients obtained for CH<sub>4</sub> being  $d = -0.009974 \text{ pph}^{-1}$  and  $e = -0.0001757 \text{ pph}^{-2}$ .

As requested by one of the referees, we discuss here the reported sensitivity of the CRDS pressure sensor with H<sub>2</sub>O by Reum et al. (2019). First of all, we point out that we have found the fits of the standard H<sub>2</sub>O correction models (Eqs. 12 and 13) to our empirical data to be excellent (see Figs. 10 and B1). Note that we have used a long water-droplet test instead of the common short droplet test used by Reum et al. (2019). Those authors also used a method that maintains stable water vapor levels but only considers a discrete set of levels. Since they also found a large disparity of results between different units of the same CRDS model, we recommend further investigation into the pressure sensor sensitivity claimed by Reum et al. (2019), taking into account the following two facts. First, when attaching the external pressure measurement unit (Fig. 2 of Reum et al., 2019), the choked

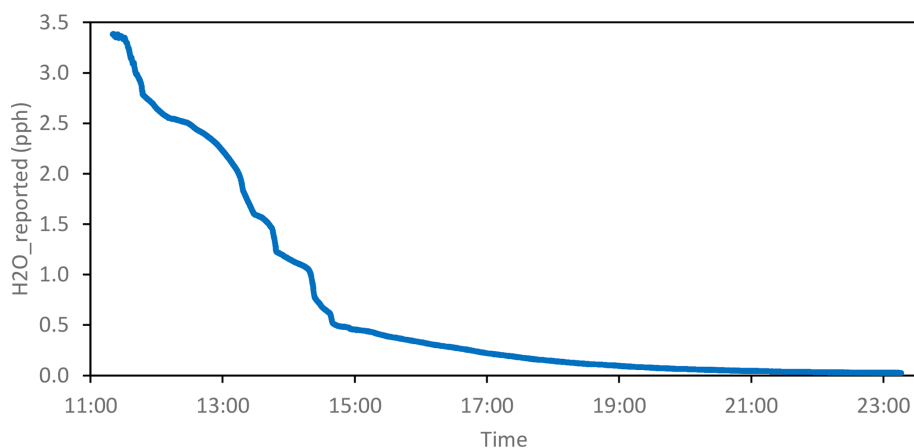


**Figure 9.** Evolution in time of the  $h2o\_reported$  (pph) determined by the CRDS.

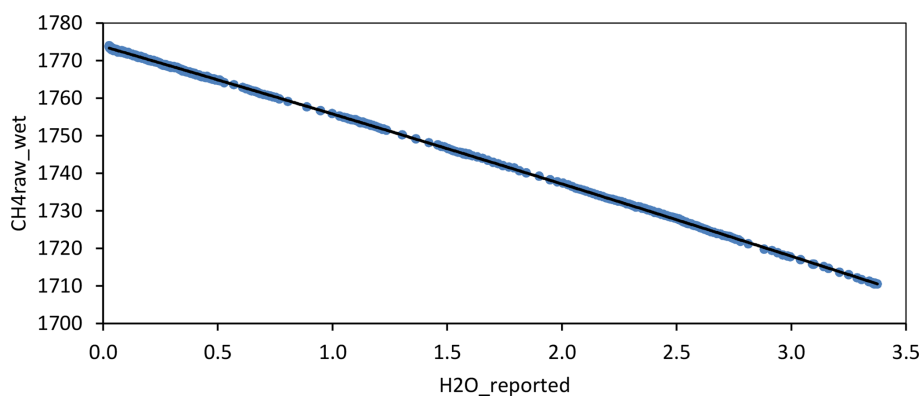


**Figure 10.**  $CH4raw\_wet$  vs.  $hr$  during the water-droplet experiment (in blue) and the least-square fitted curve (in black).

flow takes place at the needle valve called “choke” instead of at the CRDS outlet valve. However, at the CRDS outlet valve, which has a critical orifice in the flight-ready CRDS used by those authors, there is a significant longitudinal decrease in the pressure due to viscosity. Note that if the CP is increased, the flow rate increases (see our Eq. 2, but using CP instead of  $p_i$ ), and the pressure drop due to viscosity increases. This seems to be indeed the reason that explains the 0.95 value those authors found for the derivative of the external pressure with respect to the CRDS pressure. Note also that humid air has a larger dynamical viscosity than dry air (e.g., Tsilingiris, 2008). For the H<sub>2</sub>O mole fraction between 0 and 5 pph, it holds that dynamical viscosity depends almost linearly on the H<sub>2</sub>O mole fraction, being equal at 45 °C to  $1.94 \times 10^{-5} \text{ N s m}^{-2}$  for 0 pph, whereas it is equal to  $2.04 \times 10^{-5} \text{ N s m}^{-2}$  for 5 pph (obtained from the Tsilingiris, 2008, equations). This fact agrees in sign with the 1 % decrease reported by Reum et al. (2019) on the derivative of the external pressure with respect to the CRDS pressure when considering humid air (3 pph). Second, on the tee to which the external pressure sensor is attached, there is a H<sub>2</sub>O gradient between the main flow and the dryer, and a net H<sub>2</sub>O

diffusive flux from the main flow till the dryer, which might produce a drag force in the dry air. Then, this dry air would need to adopt a configuration with a pressure gradient force opposing the H<sub>2</sub>O drag force. This would mean that the external pressure sensor would measure a pressure larger than that presented in the main flow, and the pressure difference would increase with the H<sub>2</sub>O mole fraction.

We consider here briefly, in order to suggest future research on this topic, a fact that has not been taken into account in the previous CRDS literature according to our knowledge. Due to the CRDS inlet critical orifice, at the same time as the velocity increases until it becomes supersonic, there is an adiabatic expansion of the air that decreases the temperature below the dew/frost point if the air has enough water vapor. Note that at the critical orifice the velocity becomes sonic, the pressure is 0.528 times the inlet pressure, the density is 0.634 times the inlet density, and the absolute temperature is 0.833 the inlet absolute temperature (Courant and Friedrichs, 1976). Those values decrease more downstream of the critical orifice till the air reaches the stationary shock front, where the velocity decreases suddenly and the temperature increases suddenly until reaching a value simi-

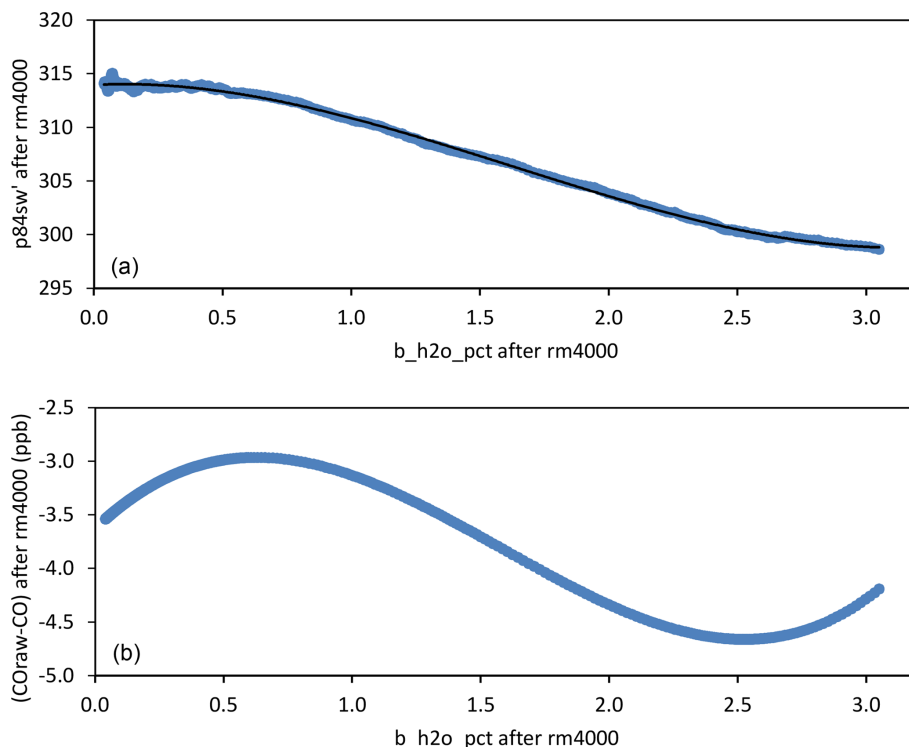


**Figure 11.** (a)  $p84sw'$  vs.  $bh$  during the water-droplet experiment (blue dots), both after performing a 4000-data running mean, and the least-square fitted curve corresponding to Eq. (15) in black. (b) Difference between the raw CO provided by the CRDS and the CO processed in the way described in this article (including H<sub>2</sub>O correction and calibration), both after performing a 4000-data running mean.

lar to the inlet one (Courant and Friedrichs, 1976). We suggest future research on the following possibility: formation of micro-droplets in the expansion flow, dissolution of CO<sub>2</sub> in these micro-droplets, and interchange of oxygen atoms between the dissolved CO<sub>2</sub> and the liquid water (therefore, the isotopic ratios are changed), before the micro-droplets are suddenly evaporated at the shock front.

For CO, we rely on the H<sub>2</sub>O dilution and pressure broadening correction determined by Rella (2010), as other authors have done (Chen et al., 2013; Oliver Laurent, private communication, 2017), and determine an improvement in the correction for the CO peak interference (zero error or spectral-baseline correction) due to the nearby H<sub>2</sub>O peak, with respect to the factory values. To this end, we use a simple and accurate novel method. We consider the equation

$$p84sw' + A \cdot bh + B \cdot bh^2 + C \cdot bh^3 = p84sd' \cdot (1 + d \cdot bh + e \cdot bh^2), \quad (14)$$

which is equivalent to Eqs. (12) and (13) except for the cubic polynomial on the left-hand side that accounts for the mentioned CO spectral-baseline correction. We advance that the novelty is not in the cubic correction (Chen et al., 2013; Karion et al., 2013, used a quartic correction), but in the method described below. We use  $d = -0.01287$  and  $e = -0.0005365$  (Rella, 2010), and  $p84sd'$ ,  $A$ ,  $B$ , and  $C$  are

determined by least-square fitting of the experimental data to the cubic equation

$$p84sw' = p84sd' + (d \cdot p84sd' - A) \cdot bh + (e \cdot p84sd' - B) \cdot bh^2 - C \cdot bh^3, \quad (15)$$

obtained rearranging Eq. (14). The instantaneous CRDS CO signal is quite noisy, but the noise is significantly reduced by using 4000-data running means (39.2 min approximately) without compromising the accuracy of the data due to the long duration of the experiment. Note that least-square fits are very sensitive to outliers, and the fit will be more accurate if the 4000-data running mean is performed previously (using a 39 min running mean instead of a 1 min running mean, the random noise is reduced by a factor of 6, approximately). As far as the authors know, this is new in the GHG monitoring literature. It is important to have a very accurate H<sub>2</sub>O correction, since in spite of the fact that the instantaneous CRDS CO values are quite noisy, such noise decreases significantly when performing successively 30 s, 1 h, 12 h means, whereas the hypothetical error in the H<sub>2</sub>O correction remains constant, behaving as a bias. After performing the 4000-data running means, we aggregate data computing 100-data means as for CO<sub>2</sub> and CH<sub>4</sub>. Figure 11 shows  $p84sw'$  vs.  $bh$  during the experiment and the least-square fitted curve corresponding to Eq. (15).

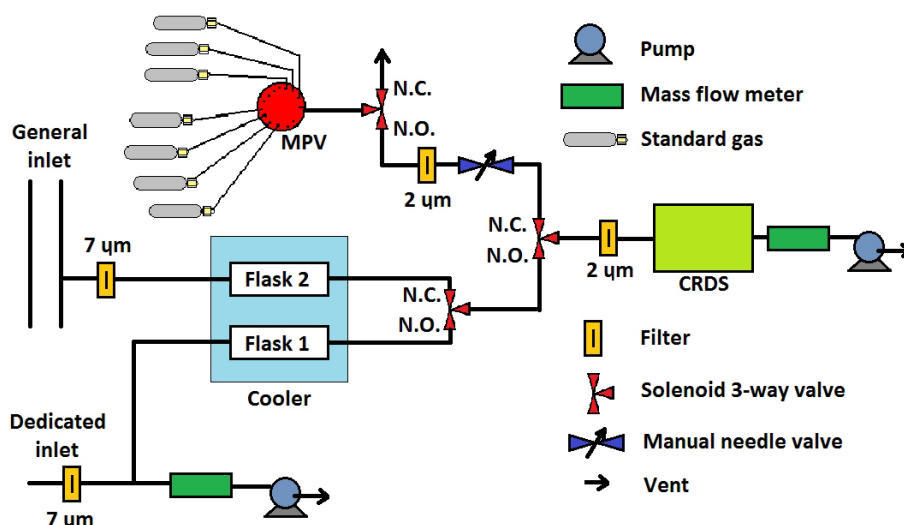


Figure 12. Ambient air/gas standard plumbing configuration operational since 28 November 2016.

After determining the coefficients of that cubic polynomial, we solve for the unknown constants in Eq. (14):  $A = -5.287565 \text{ raw ppb}^{-1}$ ,  $B = 5.283987 \text{ raw ppb}^{-2}$ , and  $C = -1.120169 \text{ raw ppb}^{-3}$ . The absolute value of  $A$  is much smaller than  $1000 \times |w_1|$ , which appears in Eq. (5). This means  $A$  is indeed a relatively small correction. By contrast,  $B$  and  $C$  are very significant corrections compared with their respective terms in Eq. (5), in which there is no cubic term. Figure 11 also shows the difference between the raw CO provided by the CRDS and the CO processed in the way described in this article (including H<sub>2</sub>O correction and calibration), both after performing a 4000-data running mean. The difference of  $-3.5 \text{ ppb}$  at the intercept is due to the calibration ( $CO_{\text{raw}}$  is not calibrated), whereas the “sinusoidal” behavior in  $bh$  is due to the different spectral-baseline correction, which in the first variable is generic, whereas in the second variable it is specific to our CRDS unit.

## 6 Ambient measurements

Figure 12 shows the ambient air/gas standard plumbing configuration operational since 28 November 2016. Before that date, there was no “dedicated inlet”, no drying (no cooled flasks), no solenoid or needle valves, and ambient air entered through the MPV. Operational ambient air measurements started on 27 November 2015. Target gas measurements started on 18 December 2015 with a 7 h cycle (3 h of ambient, 30 min of target 1, 3 h of ambient, and 30 min of target 2) to monitor better the behavior of the CRDS, which became a 21 h cycle after 24 June 2016. With the new plumbing configuration, ambient air is alternatively sampled from the two inlet lines within the 21 h cycle (15 h of ambient from the dedicated inlet and 5 h of ambient from the general inlet). This has two purposes: (1) to provide plenty of time to ex-

change the flask used to trap H<sub>2</sub>O in the air line not used at this moment; (2) to check the consistency between both lines after every switch: a bias between them might indicate the existence of a leak in one of the lines (e.g., in the general inlet, which has a few large unions and several instruments connected to it; or at the flasks connections). Since the cooler bath temperature is  $-40 \text{ }^\circ\text{C}$ , there is no complete drying. Therefore, it has been necessary to apply the water vapor correction for the full measurement period.

### 6.1 Ambient air measurement processing

After performing the pre-processing detailed in Sect. 3, we apply an additional filtering to the 30 s means. We retain a pre-processed 30 s mean if the following conditions are met: (1) the mean values of the following variables are within the indicated ranges: CP:  $186.7 \pm 0.047 \text{ hPa}$  ( $140 \pm 0.035 \text{ Torr}$ ), CT:  $45 \pm 0.02 \text{ }^\circ\text{C}$ , and OV: 20 000–40 000; (2) there is a calibration before and after the ambient mean considered, distant in time less than 180 days from each other, as is done in ICOS (Hazan et al., 2016).

Then, we apply the following processing scheme. Firstly, we apply water vapor correction: (a) using Eqs. (12) and (13) we compute  $CO_{2\text{ovc\_dry}}$  and  $CH_{4\text{raw\_dry}}$  from  $CO_{2\text{ovc\_wet}}$ ,  $CH_{4\text{raw\_wet}}$  and  $hr$  (i.e., dilution and pressure broadening effect correction); (b) using Eq. (14) we compute  $p_{84sd'}$  from  $p_{84sw'}$  and  $bh$  (i.e., refinement of the interference correction as well as dilution and pressure broadening effect correction). Secondly, we apply the calibration curves interpolated linearly in time: (a) for CO<sub>2</sub>, we employ Eq. (9) using  $CO_{2\text{ovc\_dry}}$  where it says  $CO_{2\text{ovc}}$ ; (b) for CH<sub>4</sub>, we employ Eq. (6) using  $CH_{4\text{raw\_dry}}$  where it says  $CH_{4\text{raw}}$ ; and (c) for CO, we employ Eq. (7) using  $p_{84sd'}$  where it says  $p_{84sw'}$ . Finally, we proceed to discard data due to the stabilization time after any sample path switch: 10 min for

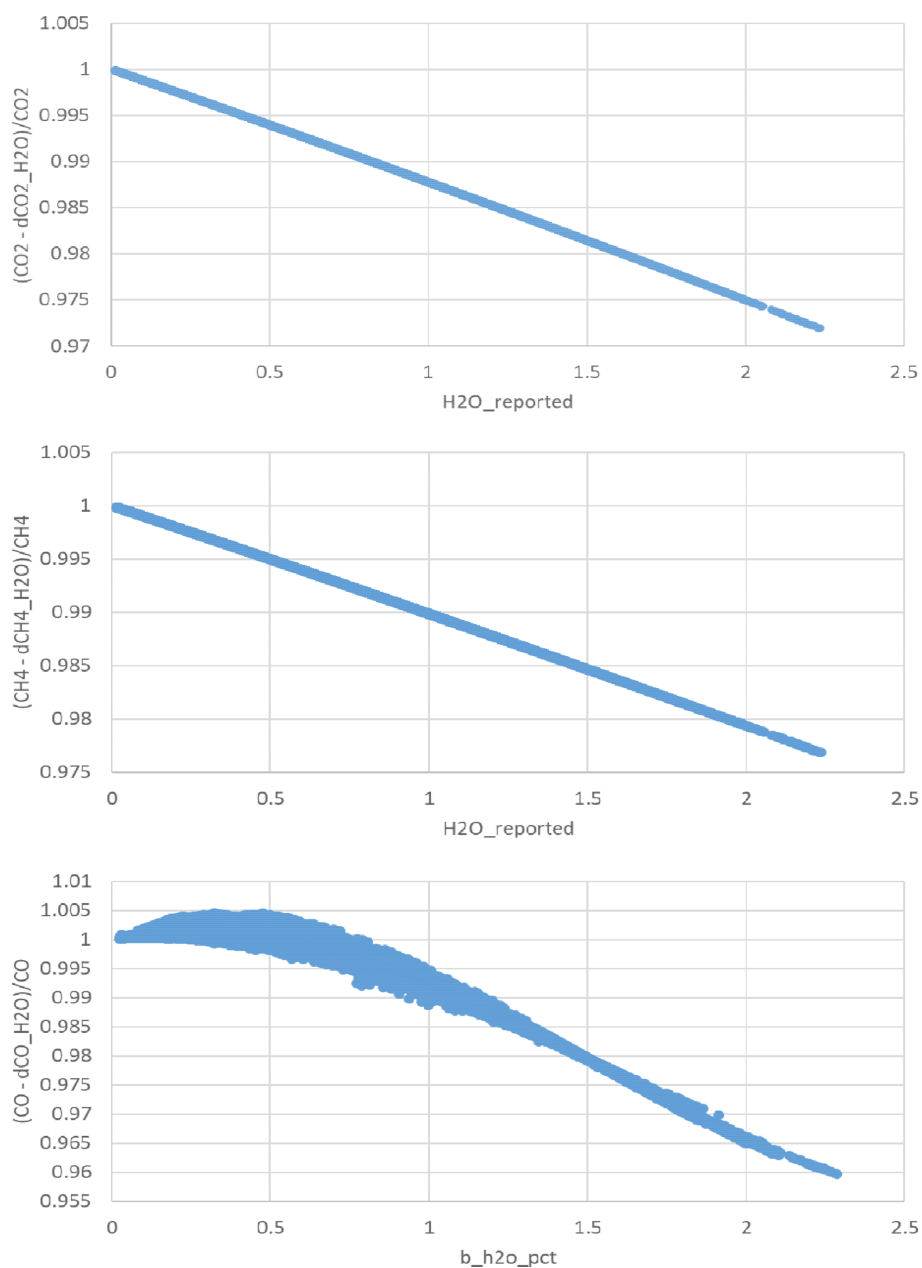


**Figure 13.** Indirect plots of the H<sub>2</sub>O corrections applied to CO<sub>2</sub> (dCO<sub>2</sub><sub>H2O</sub>), CH<sub>4</sub> (dCH<sub>4</sub><sub>H2O</sub>) and CO (dCO<sub>H2O</sub>) in physical units for ambient air measurements at IZO, e.g., dCO<sub>2</sub><sub>H2O</sub> is equal to  $(CO_2_{ovc\_dry} - CO_2_{ovc\_wet})$  divided by the local slope of the calibration curve (Eq. 8).

ambient measurements and 20 min for target and calibration gas injections.

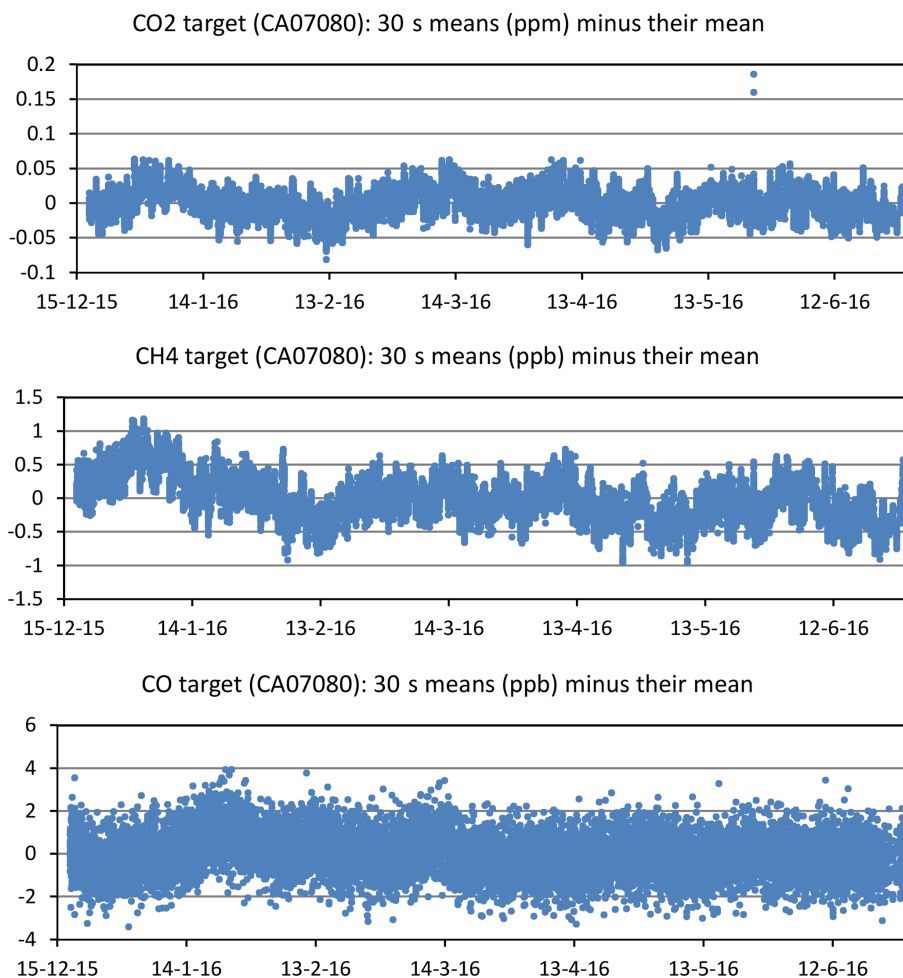
Figure 13 shows implicitly the H<sub>2</sub>O corrections applied to CO<sub>2</sub> (dCO<sub>2</sub><sub>H2O</sub>), CH<sub>4</sub> (dCH<sub>4</sub><sub>H2O</sub>) and CO (dCO<sub>H2O</sub>) in physical units for ambient air measurements at IZO, e.g., dCO<sub>2</sub><sub>H2O</sub> is equal to  $(CO_2_{ovc\_dry} - CO_2_{ovc\_wet})$  divided by the local slope of the calibration curve (Eq. 8). The plots for CO<sub>2</sub> and CH<sub>4</sub> are curves. However, the plot for CO shows a cloud of dots because Eq. (14) is more complex and

there does not exist a bijection between the  $X$  and  $Y$  variables.

After the date in which the cold bath was implemented ( $-40^\circ\text{C}$ ), the applied H<sub>2</sub>O corrections for ambient air measurements have been quite small: (1) for CO<sub>2</sub>, the mean correction has been 0.10 ppm (maximum: 0.36 ppm, minimum: 0.09 ppm; both for 10 min means); (2) for CH<sub>4</sub>, the mean correction has been 0.38 ppb (maximum: 1.39 ppb, minimum: 0.34 ppb; both for 10 min means); and (3) for CO, the mean correction has been  $-0.03$  ppb (maximum in absolute value:

**Table 6.** Statistics for the target gas injections (30 s mean assignments): mean and SD for the different species.

| Tank/months       | CO <sub>2</sub> (ppm) | SD    | CH <sub>4</sub> (ppb) | SD   | CO (ppb) | SD   |
|-------------------|-----------------------|-------|-----------------------|------|----------|------|
| CA07080/7 months  | 381.96                | 0.020 | 1825.43               | 0.32 | 148.60   | 0.97 |
| CA05038/7 months  | 368.85                | 0.020 | 1777.04               | 0.33 | 93.56    | 0.99 |
| CA06812/13 months | 372.48                | 0.020 | 1784.80               | 0.27 | 142.04   | 1.01 |
| CA05034/13 months | 363.71                | 0.020 | 1775.89               | 0.27 | 139.11   | 0.98 |

**Figure 14.** Time series of mole fraction assignments for one of the target gases.

−0.07 ppb, minimum in absolute value: −0.01 ppb; both for 10 min means). Since those corrections are quite small, for this period relying on the generic factory H<sub>2</sub>O corrections would have been sufficient.

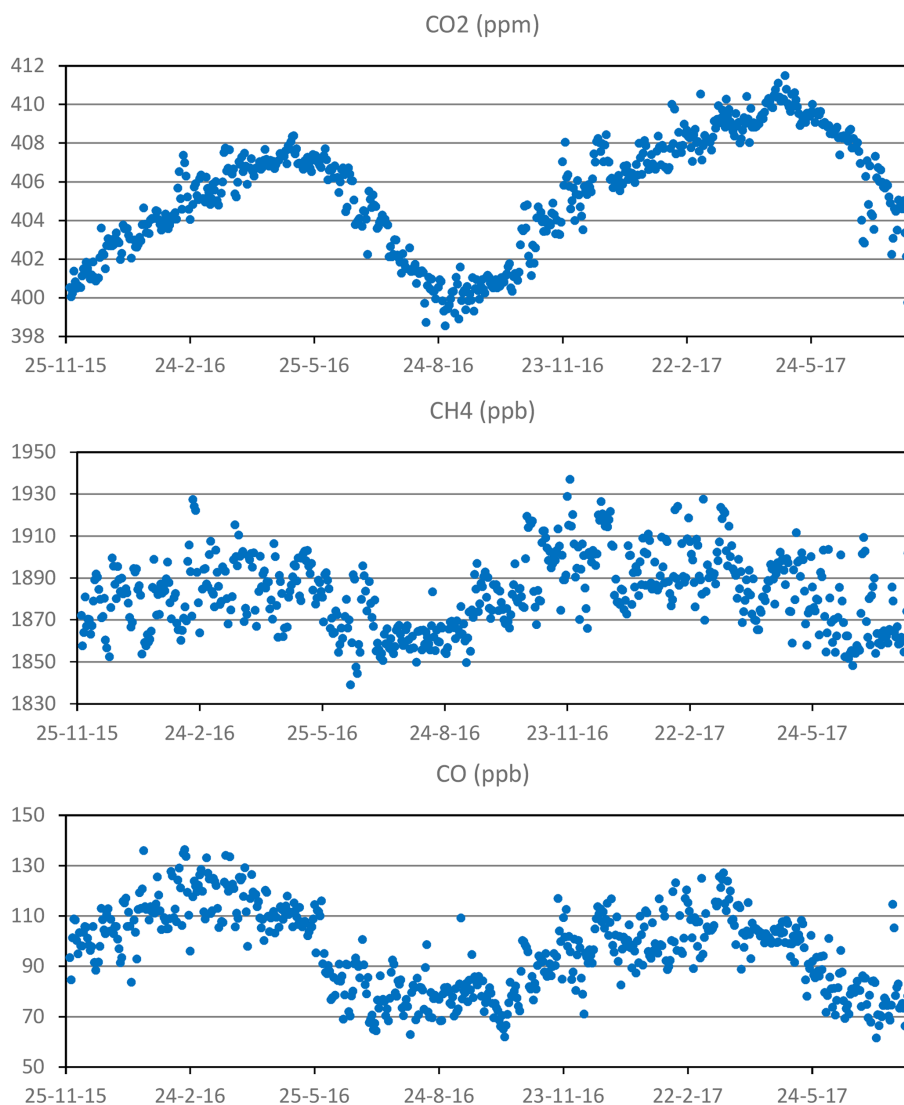
## 6.2 Target gas injections

Table 6 summarizes the statistics for the target gas injections (30 s mean assignments), whereas Fig. 14 shows the time series of mole fraction assignments for one of the target gases. The results are good. Note that 30 s is too short a time for CO, and it is necessary to consider longer averages to reduce

noise. The ambient processing scheme described in Sect. 6.1 is also used to assign mole fractions to the target and calibration gas injections, and it is checked that the water vapor correction for them is smaller than 0.01 ppm for CO<sub>2</sub>, and 0.1 ppb for CH<sub>4</sub> and CO.

## 6.3 Comparison with other continuous measurements carried out at Izaña

In this subsection, we compare the CRDS IZO ambient daily-nighttime (from 20:00 UTC of the previous day till 08:00 of the considered day) means with the co-located hourly means



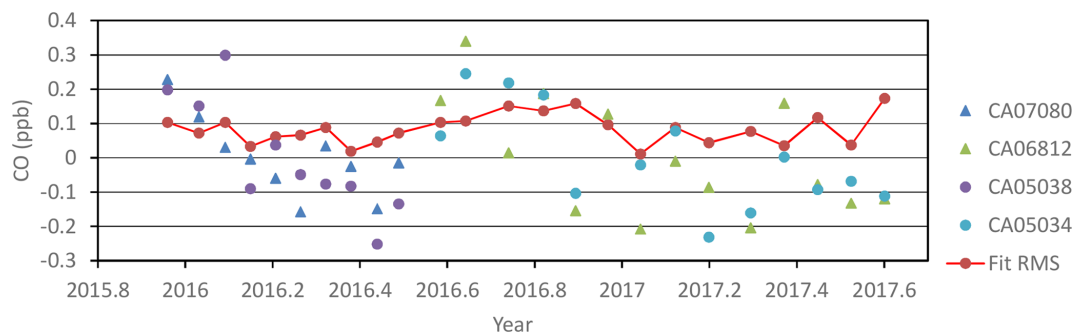
**Figure 15.** Time series of daily-nighttime (12 h averages) CRDS measurements (CO<sub>2</sub>, CH<sub>4</sub> and CO).

from the IZO Li7000 NDIR for CO<sub>2</sub> (Gomez-Pelaez et al., 2011, 2014, 2016), IZO Varian GC-FID for CH<sub>4</sub> (Gomez-Pelaez et al., 2011, 2012, 2016), and IZO RGA-3 GC-RGD for CO (Gomez-Pelaez et al., 2013, 2016), all of them in the scales already indicated in Sect. 4. We use daily-nighttime means for the comparison because (1) as mentioned in the introduction, IZO has background conditions during nighttime; and (2) when using 12 h averages, we improve the signal-to-noise ratio and remove any hypothetical dependence on the used IZO general inlet due to small inhomogeneities in space and time of the mole fraction fields. Note that the data for 2017 are still not final. Figure 15 shows the time series of daily-nighttime CRDS measurements, whereas Table 7 shows the monthly-mean differences between the daily-nighttime CRDS measurements and those for the rest of the mentioned IZO instruments. As Table 7 shows, for CO<sub>2</sub> and CH<sub>4</sub> the differences between the instruments are within the

GAW compatibility objectives (0.1 ppm for CO<sub>2</sub> and 2 ppb for CH<sub>4</sub>), except for 4 months for the former and 3 months for the latter (coincident with those for CO<sub>2</sub>). The larger differences took place in October and November 2016. We think they were produced by a small leak in the general inlet used by the CRDS (the NDIR and the GC-FID used another general inlet). However, for CO the difference between the instruments is larger than 2 ppb after March 2016. The WMO tertiary standards used in the RGA-3 have been calibrated two times by the WMO CCL and the inferred drifts were considered significant, extrapolated forward in time, and taken into account in the RGA-3 data processing. These results seem to support the hypothesis that the observed negative differences are explained by the fact that the CRDS laboratory standards (WMO tertiaries) might be drifting up significantly for CO (see Sect. 4).

**Table 7.** Monthly-mean differences between the daily-nighttime CRDS measurements and those for the rest of the mentioned IZO instruments (Li7000 NDIR for CO<sub>2</sub>, Varian GC-FID for CH<sub>4</sub>, and RGA-3 GC-RGD for CO).

| Year        | Month | CO <sub>2</sub> CRDS –<br>CO <sub>2</sub> Li7000 (ppm) | CH <sub>4</sub> CRDS –<br>CH <sub>4</sub> VarianFID (ppb) | CO CRDS –<br>CO RGA3 (ppb) |
|-------------|-------|--|---|----------------------------|
| Full period |       | –0.07  | 1.2   | –2.8                       |
| 2015        | 11    | –0.08  | 1.6   | –0.4                       |
| 2015        | 12    | –0.04  | 0.9   | –1.1                       |
| 2016        | 1     | –0.03  | 1.0   | –1.3                       |
| 2016        | 2     | –0.08  | 1.0   | –1.8                       |
| 2016        | 3     | –0.07  | 0.3   | –2.4                       |
| 2016        | 4     | –0.06  | –0.1  | –2.7                       |
| 2016        | 5     | –0.02  | 0.2   | –2.9                       |
| 2016        | 6     | –0.03  | 0.9   | –3.0                       |
| 2016        | 7     | 0.00   | 1.1   | –3.2                       |
| 2016        | 8     | 0.05   | 1.9   | –2.9                       |
| 2016        | 9     | –0.10  | 2.0   | –3.1                       |
| 2016        | 10    | –0.12  | 3.3   | –4.1                       |
| 2016        | 11    | –0.15  | 3.1   | –3.0                       |
| 2016        | 12    | –0.07  | 0.5   | –3.7                       |
| 2017        | 1     | –0.09  | 1.1   | –3.0                       |
| 2017        | 2     | –0.14  | 2.1   | –3.3                       |
| 2017        | 3     | –0.11  | 0.5   | –3.6                       |
| 2017        | 4     | –0.08  | 0.4   | –2.7                       |
| 2017        | 5     | –  | 0.3   | –3.4                       |

**Figure 16.** The rms residual of the fit (red dots/line), and difference between the assigned mole fraction to a target gas and the mean mole fraction of such a target gas (a different color is used for each target gas), for each species and mole-fraction calibration performed using four WMO laboratory standards (every 3 or 4 weeks), after taking into account the drift rates of the CRDS standards.

## 7 Preliminary independent assessment on the drift rates of the CRDS CO standards

The evidence presented in Sects. 4 and 6.3 seem to indicate the CRDS CO WMO tertiary standards might be drifting significantly. These standards have been calibrated only once by CCL: in August–September 2015. In order to perform a preliminary independent assessment on the drift rates of the CRDS CO standards, we have proceeded as follows. As mentioned in Sect. 6.3, the WMO tertiary standards used in the RGA-3 have been calibrated twice (9 years distant) by the WMO CO CCL and the inferred drifts were considered significant and extrapolated forward in time. We have performed

a four-cycle calibration in the CRDS to compare the CRDS standards (CB11240, CB11389, CB11393, and CB11340) and the RGA-3 standards (CA06968, CA06768, CA06988, CA06946, and CA06978). The first step has been assigning CO<sub>2</sub> and CH<sub>4</sub> mole fractions to the RGA-3 standards using the calibration curves obtained using the CRDS standards. The second step has been assigning CO mole fractions to the CRDS standards using the calibration curve obtained using the RGA-3 standards, whose fit rms residual is 0.4 ppb. In the third step, we determined the drift rate of each CRDS standards using the CCL assignment done in 2015 and the present assignment (done on 4 October 2017), which is indirectly traceable to the WMO primaries. The CB11240 standard is

the only one with a significant drift rate,  $1.21 \text{ ppb year}^{-1}$ , with 195.87 ppb at present. The other three standards all have positive drift rates, with the maximum being  $0.17 \text{ ppb year}^{-1}$ . We have performed the exercise of reprocessing all the CRDS calibrations taking into account the drift rates determined for the four CRDS standards (even those which are not statistically significant), as shown in Fig. 16. Comparing Fig. 16 with Fig. 7c, we see now that there is no trend in the rms residual from the calibration fit, and the downward drift of the target gases is significantly smaller. However, when reprocessing the CRDS ambient CO time series, the maximum improvement in the CRDS minus RGA-3 monthly difference time series is 0.3 ppb for some periods, remaining unchanged the global mean difference for the full period. Therefore, we infer the performance of the calibrations improves largely when taking into account the quite significant drift in the standard CB11240, but the CRDS vs. RGA-3 ambient differences remain almost unchanged. Perhaps, a possible explanation might be in the problems detected recently by the CCL in the CO WMO-X2014A scale ([https://www.esrl.noaa.gov/gmd/ccl/co\\_scale\\_update.html](https://www.esrl.noaa.gov/gmd/ccl/co_scale_update.html), last access: 26 March 2019).

## 8 Summary and conclusions

At the end of 2015, a CO<sub>2</sub>/CH<sub>4</sub>/CO CRDS was installed at the Izaña Global GAW station to improve the Izaña GHG GAW Measurement Programme and guarantee its long-term maintenance. The CRDS passed the acceptance tests. However, a correction for CO<sub>2</sub> that takes into account the inlet pressure had to be incorporated in order to achieve a rms residual of around 0.02 ppm, which is the value we obtain with the IZO NDIR-based measurement systems. For CO, our data processing is based on the raw spectral peak data instead of on the raw CO provided by the instrument. The relationships between flow rate, CRDS inlet pressure, and CRDS outlet valve aperture have been determined also. The CRDS inlet pressure sensitivity is determined for the different compounds as well as its stability over the years.

We use linear response functions for CH<sub>4</sub> and CO, and a quadratic response function for CO<sub>2</sub>. The CRDS long-term drift of the raw responses is  $0.104 \text{ ppm year}^{-1}$  for CO<sub>2</sub>,  $2.22 \text{ ppb year}^{-1}$  for CH<sub>4</sub>, and  $0.544 \text{ ppb year}^{-1}$  for CO. Assuming that those drifts are due to drifts in the real pressure and temperature of the cavity, we have determined that our CRDS has a long-term drift of  $0.0678 \text{ }^\circ\text{C year}^{-1}$  and  $0.595 \text{ hPa year}^{-1}$  in the cavity sensors using relations between partial derivatives. We also show the evolution in time of the response-function local slopes at the mole fractions of the virtual tank, as well as the rms residual in the calibration fits, which has no significant trend except for CO.

The time series of target gas assignments during calibrations are also shown, which again indicate a good behavior for CO<sub>2</sub> and CH<sub>4</sub> but a downward drift for CO. Those facts

suggest the CRDS CO WMO tertiary standards are probably drifting significantly in spite of the fact that they have only been used during 2 years. Using an independent set of CO laboratory standards whose drift rates have been determined by the CO CCL, we conclude that one of the CRDS standards is drifting quite significantly ( $1.21 \text{ ppb year}^{-1}$ ). The performance in the calibrations improves when taking that drift into account.

The results of the long water-droplet test (12 h) have been presented and used for the H<sub>2</sub>O water vapor correction. The determination of the H<sub>2</sub>O correction for CO presents two novelties: use of the raw spectral peak data and use of a running mean to smooth random noise before performing the least square fit.

We have presented the ambient measurement scheme and its data processing. Target gas injections show very small standard deviations except for CO. The agreement with other IZO in situ continuous measurements is good most of the time for CO<sub>2</sub> and CH<sub>4</sub>, but for CO is just outside the GAW 2 ppb objective. It seems the disagreement is not produced by the drifts in the CRDS CO WMO tertiary standards. The mean differences for the full period are  $-0.07 \text{ ppm}$  for CO<sub>2</sub>,  $1.2 \text{ ppb}$  for CH<sub>4</sub>, and  $-2.8 \text{ ppb}$  for CO.

We have determined and discussed the physical origin of the inlet pressure and H<sub>2</sub>O dependences of the CRDS flow, and pointed out the existence of flow-rate-dependent small spatial inhomogeneities in the pressure and temperature fields inside the cavity. We have shown that the regions slightly depleted in pressure inside the CRDS cavity in the neighborhood of the inlet and outlet pipes, due to the cross-sectional change, are probably the cause of the slight CO<sub>2</sub> correction associated with the mass flow rate we have empirically obtained. We suggest performing a gas dynamic numerical simulation of the pressure and temperature fields inside the CRDS cavity for different flow rates. This could help to improve the spectral forward model used by the CRDS and also to take into account more accurately the impact of the flow rate on the measurements. Furthermore, the use of conical adapters for connecting the pipes to the CRDS cavity might keep the pressure gradients associated with the cross-sectional changes out of the laser path.

*Code and data availability.* The Fortran 90 codes developed in this work could be made available to other researchers under a cooperative agreement with the Izaña Atmospheric Research Centre (AEMET). However, a very limited support on their use could be provided.

The data presented in this paper is available under request. If the supplied data is intended to be used in a scientific article, co-authorship should be offered to data providers.

### Appendix A: A note concerning the H<sub>2</sub>O dependence of the CRDS flow and the spatial inhomogeneity of the pressure field inside the cavity

The theoretical equation relating the standard volumetric flow ( $F$ ) to the inlet quantities for a choked flow is presented and discussed in Sect. 2.4. However, additionally to the dependences on pressure and temperature, there is also a small dependence on the water vapor mole fraction through the ratio of specific heats and the gas constant, which depend slightly on the H<sub>2</sub>O mole fraction as follows:

$$\frac{1}{R} = \frac{1-r}{R_d} + \frac{r}{R_{\text{H}_2\text{O}}}, \quad (\text{A1})$$

where  $r$  is the H<sub>2</sub>O mole fraction in mol mol<sup>-1</sup>,  $R_d$  is the gas constant for dry air, and  $R_{\text{H}_2\text{O}}$  is the gas constant for H<sub>2</sub>O;

$$\gamma = \frac{1.4 + 0.4 \cdot r}{1 + 0.4 \cdot r}. \quad (\text{A2})$$

In order to estimate the relative impact of water vapor changes on the standard volumetric flow, we need to know approximately the values of  $C_d$  and  $A$ . To this end, we use this fact obtained from Table 3, when  $p_i$  is 700 hPa,  $F$  is 150 scc min<sup>-1</sup>, and obtain using Eq. (2) that the product of  $C_d$  and  $A$  is equal to  $1.955 \times 10^{-8}$  m<sup>2</sup>. Figure A1 shows  $F$  and its derivative (with respect to  $r$ ) as functions of  $r$ , for  $p_i = 700$  hPa and  $T_i = 293$  K, showing that the relative impact of  $r$  on  $F$  is small and the derivative is quite constant for the considered  $r$  range (0.00–0.05).

When there is a stationary air flow through an instrument, the pressure field changes spatially mainly for two reasons (Bernoulli equation): (1) longitudinal decrease in the pressure due to viscosity, and (2) changes in the cross section along the pipe, which require flow acceleration (provided by a longitudinal pressure gradient) when the cross section decreases and flow deceleration when the cross section increases (e.g., Venturi effect). The structure of the optical cavity of the CRDS G2401 is shown in Fig. 1 of Crosson (2008). The plane defined by the three mirrors inside the cavity is horizontal (parallel to the surface of the Earth when the instrument is set on its feet on a bench). The inlet and outlet cavity ports are on the top of the cavity. The pressure sensor is on a third port located on the top of the cavity, at the approximate center (Chris Rella, personal communication, 2017). Applying considerations of fluid dynamics, we infer the following facts. First, along the sense of flow inside the cavity, there needs to be a very small decrease in pressure in order to be able to balance the resistance to flow due to viscosity, and that decrease will be larger as the mass flow rate is increased. Since the pressure sensor is located in the middle of the cavity, the mean pressure will be monitored. A parcel of fluid flowing along the cavity will expand very slightly (due to the decrease in pressure that the Lagrangian parcel experiences), and therefore, the temperature will tend

to slightly decrease adiabatically in all the points of the volume, whereas the heat to compensate it comes from the surface of the cavity. That is, necessarily there needs to also be a small inhomogeneity in the temperature field inside the cavity, and this inhomogeneity depends on the flow rate. The hypothetical net effect on the measurements is difficult to assess a priori without performing a gas dynamics numerical simulation. Second, when a fluid parcel leaves the inlet pipe and enters into the cavity, it experiences a large change in the cross section of the solid material that contents the flow. Therefore, there needs to be a portion of cavity near the inlet with pressure increasing in the flow sense to decrease and accommodate the velocity of the fluid. That is, in the cavity near the inlet, there is a pressure smaller than in the rest of the cavity. Moreover, the opposite process happens in the cavity near the outlet: the fluid needs to be accelerated, and therefore, there needs to be a portion of cavity near the outlet with pressure decreasing in the flow sense. That is, in the cavity near the outlet, there is a smaller pressure than in the rest of the cavity, as happens near the inlet, and this decrease is larger when the mass flow rate is increased. If any portion of those two regions is crossed by the laser path, the perturbation this produces in the measurements agrees in sign with Eq. (3). Therefore, this might be the explanation of the empirically observed effect described in Sect. 3.1.

All the effects pointed out in this Appendix are new in the GHG measurement literature according to the knowledge of the authors.

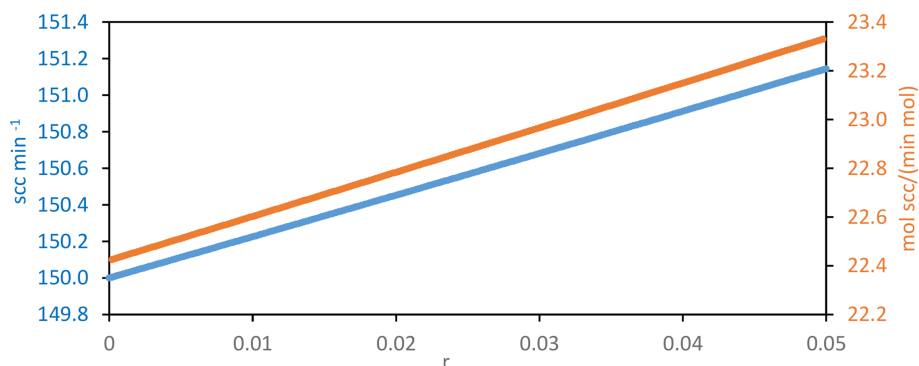


**Figure A1.** Standard volumetric flow ( $F$ ) on the left y axis and its derivative with respect to  $r$  ( $\text{H}_2\text{O}$  mole fraction in  $\text{mol mol}^{-1}$ ) on the right y axis, for  $p_i = 700$  hPa and  $T_i = 293$  K.

### Appendix B: $\text{CO}_2\text{ovc\_raw}$ vs. $hr$ during the water-droplet experiment

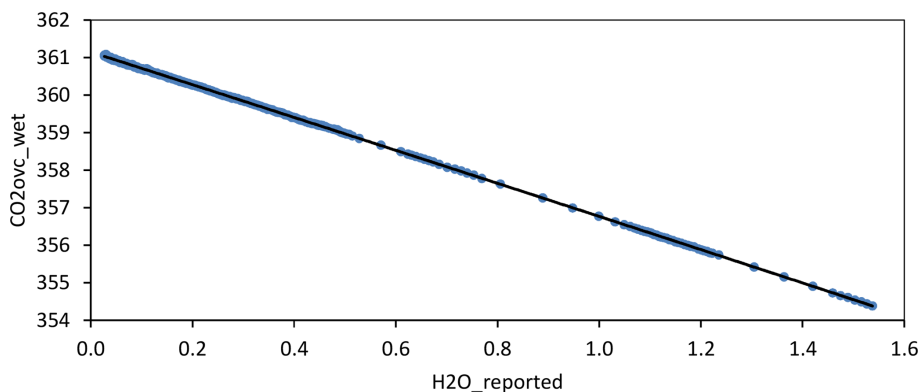


**Figure B1.**  $\text{CO}_2\text{ovc\_raw}$  vs.  $hr$  during the water-droplet experiment (in blue) and the least-square fitted curve (in black), where only the 0.0–1.55  $hr$  range has been plotted.

### Appendix C: Some additional novelties in the Izaña GHG instrumentation since GGMT-2015

We have introduced the following improvements in the dedicated inlet lines of the IZO GHG measurement systems since GGMT-2015: (1) backpressure regulators for the vents located downstream of the pumps, and rotameters for those vents; (2) needle valves in low flow vents installed downstream of the cryotraps; (3) glass flask cryotraps with Ultra-Torr connections; and (4) hermetic plugs for unused ports of the rotary Valco valves.

We have prepared two CO<sub>2</sub> laboratory standards of 418.7 ppm for Izaña NDIRs Li7000 and Li6252 (using two cylinders that have proved to be very stable in previous uses as CO<sub>2</sub> working standards), and calibrated them against our CRDS WMO laboratory standards using the G2401 CRDS.

We have reprocessed the Izaña time series of CH<sub>4</sub> and CO in scales X2004A and X2014A, respectively, also taking into account the drift of the five WMO laboratory standards used in Izaña RGA-3.

*Author contributions.* AJGP designed the measurement system, measurement scheme, and response functions, performed the CRDS acceptance tests, configured the CRDS, determined the relationships between flow rate, OV, and CRDS inlet pressure, as well as its impact in the CRDS measurements, performed the H<sub>2</sub>O droplet tests, wrote the numerical codes, analyzed the data, made the study of Appendix A, wrote the manuscript, and drew the plots. RR installed the measurement system, helped in the routine operation of the system, revised the manuscript, and performed the additional inlet pressure sensitivity tests carried out in 2018. EC was the PI of the financed R+D infrastructure project by which the CRDS equipment could be purchased and installed at IZO, and revised in detail the manuscript. VGT performed the routine calibrations, and helped perform the additional inlet pressure sensitivity tests carried out in 2018. ER provided support configuring the CRDS computer, prepared the external media necessary to perform daily copies of the acquired data, and revised the manuscript.

*Competing interests.* The authors declare that they have no conflict of interest.

*Special issue statement.* This article is part of the special issue “The 10th International Carbon Dioxide Conference (ICDC10) and the 19th WMO/IAEA Meeting on Carbon Dioxide, other Greenhouse Gases and Related Measurement Techniques (GGMT-2017) (AMT/ACP/BG/CP/ESD inter-journal SI)”. It is a result of the 19th WMO/IAEA Meeting on Carbon Dioxide, Other Greenhouse Gases, and Related Measurement Techniques (GGMT-2017), Empa Dübendorf, Switzerland, 27–31 August 2017.

*Acknowledgements.* The acquisition of the instrument was largely financed by European ERDF funds through Spanish R+D infrastructure project AEDM15-BE-3319 of the Spanish Ministerio de Economía, Industria y Competitividad. This study was developed within the Global Atmospheric Watch (GAW) Programme at the Izaña Atmospheric Research Centre, financed by AEMET. We thank Chris Rella (Picarro, Inc., USA), Christoph Zellweger (EMPA, Switzerland), and Olivier Laurent (ICOS ATC/LSCE, France) for providing information of great interest about the Picarro G2401 CRDS, and to the Izaña observatory staff. We acknowledge the constructive comments of the anonymous referees.

*Review statement.* This paper was edited by Brigitte Buchmann and reviewed by three anonymous referees.

## References

Chen, H., Winderlich, J., Gerbig, C., Hofer, A., Rella, C. W., Crosson, E. R., Van Pelt, A. D., Steinbach, J., Kolle, O., Beck, V., Daube, B. C., Gottlieb, E. W., Chow, V. Y., Santoni, G. W., and Wofsy, S. C.: High-accuracy continuous airborne measurements of greenhouse gases (CO<sub>2</sub> and CH<sub>4</sub>) using the cavity ring-

- down spectroscopy (CRDS) technique, *Atmos. Meas. Tech.*, 3, 375–386, <https://doi.org/10.5194/amt-3-375-2010>, 2010.
- Chen, H., Karion, A., Rella, C. W., Winderlich, J., Gerbig, C., Filges, A., Newberger, T., Sweeney, C., and Tans, P. P.: Accurate measurements of carbon monoxide in humid air using the cavity ring-down spectroscopy (CRDS) technique, *Atmos. Meas. Tech.*, 6, 1031–1040, <https://doi.org/10.5194/amt-6-1031-2013>, 2013.
- Chevallier, F., Ciais, P., Conway, T. J., Aalto, T., Anderson, B. E., Bousquet, P., Brunke, E. G., Ciattaglia, L., Esaki, Y., Frohlich, M., Gomez, A., Gomez-Pelaez, A. J., Haszpra, L., Krummel, P. B., Langenfelds, R. L., Leuenberger, M., Machida, T., Maignan, F., Matsueda, H., Morgui, J. A., Mukai, H., Nakazawa, T., Peylin, P., Ramonet, M., Rivier, L., Sawa, Y., Schmidt, M., Steele, L. P., Vay, S. A., Vermeulen, A. T., Wofsy, S., and Worthy, D.: CO<sub>2</sub> surface fluxes at grid point scale estimated from a global 21 year reanalysis of atmospheric measurements, *J. Geophys. Res.*, 115, D21307, <https://doi.org/10.1029/2010JD013887>, 2010.
- Courant, R. and Friedrichs, K. O.: *Supersonic flow and shock waves*, Springer-Verlag, New York, 1976.
- Crosson, E. R.: A cavity ring-down analyzer for measuring atmospheric levels of methane, carbon dioxide, and water vapor, *Appl. Phys. B-Lasers O.*, 92, 403–408, 2008.
- Cuevas, E., González, Y., Rodríguez, S., Guerra, J. C., Gómez-Peláez, A. J., Alonso-Pérez, S., Bustos, J., and Milford, C.: Assessment of atmospheric processes driving ozone variations in the subtropical North Atlantic free troposphere, *Atmos. Chem. Phys.*, 13, 1973–1998, <https://doi.org/10.5194/acp-13-1973-2013>, 2013.
- Cuevas, E., Milford, C., Bustos, J. J., del Campo-Hernández, R., García, O. E., García, R. D., Gómez-Peláez, A. J., Ramos, R., Redondas, A., Reyes, E., Rodríguez, S., Romero-Campos, P. M., Schneider, M., Belmonte, J., Gil-Ojeda, M., Almansa, F., Alonso-Pérez, S., Barreto, A., González-Morales, Y., Guirado-Fuentes, C., López-Solano, C., Afonso, S., Bayo, C., Berjón, A., Bethencourt, J., Camino, C., Carreño, V., Castro, N. J., Cruz, A. M., Damas, M., De Ory-Ajamil, F., García, M. I., Fernández-de Mesa, C. M., González, Y., Hernández, C., Hernández, Y., Hernández, M. A., Hernández-Cruz, B., Jover, M., Kühl, S. O., López-Fernández, R., López-Solano, J., Peris, A., Rodríguez-Franco, J. J., Sálamo, C., Sepúlveda, E., and Sierra, M.: Izaña Atmospheric Research Center Activity Report 2012–2014, edited by: Cuevas, E., Milford, C., and Tarasova, O., State Meteorological Agency (AEMET), Madrid, Spain and World Meteorological Organization, Geneva, Switzerland, NIPO: 281-15-004-2, WMO/GAW Report No. 219, 2015.
- EMPA: System and Performance Audit of Surface Ozone, Methane, Carbon Dioxide, Nitrous Oxide, and Carbon Monoxide at the Global GAW Station Izaña, September 2013, WCC-Empa Report 13/2, 62 pp., [https://www.wmo.int/pages/prog/arep/gaw/documents/IZO\\_2013.pdf](https://www.wmo.int/pages/prog/arep/gaw/documents/IZO_2013.pdf) (last access: 26 March 2019), 2013.
- Gomez-Pelaez, A. J. and Ramos, R.: Improvements in the Carbon Dioxide and Methane Continuous Measurement Programs at Izaña Global GAW Station (Spain) during 2007–2009, in: GAW report (No. 194) of the “15th WMO/IAEA Meeting of Experts on Carbon Dioxide, Other Greenhouse Gases, and Related Tracer Measurement Techniques (Jena, Germany; 7–10 September, 2009)”, edited by: Brand, W. A., World Meteorological Organization (TD No. 1553), Geneva, 133–138, 2011.

- Gomez-Pelaez, A. J., Ramos, R., Gomez-Trueba, V., Campo-Hernandez, R., Dlugokencky, E., and Conway, T.: New improvements in the Izaña (Tenerife, Spain) global GAW station in-situ greenhouse gases measurement program, in: GAW report (No. 206) of the “16th WMO/IAEA Meeting on Carbon Dioxide, Other Greenhouse Gases, and Related Measurement Techniques (GGMT-2011) (Wellington, New Zealand, 25–28 October 2011)”, edited by: Brailsford, G., World Meteorological Organization, Geneva, 76–81, 2012.
- Gomez-Pelaez, A. J., Ramos, R., Gomez-Trueba, V., Novelli, P. C., and Campo-Hernandez, R.: A statistical approach to quantify uncertainty in carbon monoxide measurements at the Izaña global GAW station: 2008–2011, *Atmos. Meas. Tech.*, 6, 787–799, <https://doi.org/10.5194/amt-6-787-2013>, 2013.
- Gomez-Pelaez, A. J., Ramos, R., Gomez-Trueba, V., Campo-Hernandez, R., and Reyes-Sanchez, E.: Izaña Global GAW station greenhouse-gas measurement programme, Novelty and developments during October 2011–May 2013, in: GAW report (No. 213) of the “17th WMO/IAEA Meeting on Carbon Dioxide, Other Greenhouse Gases, and Related Measurement Techniques (Beijing, China, 10–14 June 2013)”, edited by: Tans, P., and Zellweger, C., World Meteorological Organization, Geneva, 77–82, 2014.
- Gomez-Pelaez, A. J., Ramos, R., Gomez-Trueba, V., Campo-Hernandez, R., Reyes-Sanchez, E.: GGMT-2015 Izaña station update: instrumental and processing software developments, scale updates, aircraft campaign, and plumbing design for CRDS, in: GAW report (No. 229) of the “18th WMO/IAEA Meeting on Carbon Dioxide, Other Greenhouse Gases, and Related Measurement Techniques (GGMT) (La Jolla, CA, USA, 13–17 September 2015)”, edited by: Tans, P. and Zellweger, C., World Meteorological Organization, Geneva, 125–131, 2016.
- Hazan, L., Tarniewicz, J., Ramonet, M., Laurent, O., and Abbaris, A.: Automatic processing of atmospheric CO<sub>2</sub> and CH<sub>4</sub> mole fractions at the ICOS Atmosphere Thematic Centre, *Atmos. Meas. Tech.*, 9, 4719–4736, <https://doi.org/10.5194/amt-9-4719-2016>, 2016.
- ICOS-ATC: ICOS Atmospheric Station Specifications, edited by: Laurent, O., version 1.2, Integrated Carbon Observation System, Atmospheric Thematic Center, available at: <https://icos-atc.lscce.ipsl.fr/filebrowser/download/27251> (last access: 26 March 2019), 2016.
- Karion, A., Sweeney, C., Wolter, S., Newberger, T., Chen, H., Andrews, A., Kofler, J., Neff, D., and Tans, P.: Long-term greenhouse gas measurements from aircraft, *Atmos. Meas. Tech.*, 6, 511–526, <https://doi.org/10.5194/amt-6-511-2013>, 2013.
- Patra, P. K., Krol, M. C., Montzka, S. A., Arnold, T., Atlas, E. L., Lintner, B. R., Stephens, B. B., Xiang, B., Elkins, J. W., Fraser, P. J., Ghosh, A., Hints, E. J., Hurst, D. F., Ishijima, K., Krummel, P. B., Miller, B. R., Miyazaki, K., Moore, F. L., Muhle, J., O’Doherty, S., Prinn, R. G., Steele, L. P., Takigawa, M., Wang, H. J., Weiss, R. F., Wofsy, S. C., and Young, D.: Observational evidence for interhemispheric hydroxyl-radical parity, *Nature*, 513, 219–223, <https://doi.org/10.1038/nature13721>, 2014.
- Rella, C. W.: Accurate and stable carbon monoxide measurements with the Picarro G2302, Picarro Report, 2010.
- Rella, C. W., Chen, H., Andrews, A. E., Filges, A., Gerbig, C., Hatakka, J., Karion, A., Miles, N. L., Richardson, S. J., Steinbacher, M., Sweeney, C., Wastine, B., and Zellweger, C.: High accuracy measurements of dry mole fractions of carbon dioxide and methane in humid air, *Atmos. Meas. Tech.*, 6, 837–860, <https://doi.org/10.5194/amt-6-837-2013>, 2013.
- Reum, F., Gerbig, C., Lavric, J. V., Rella, C. W., and Göckede, M.: Correcting atmospheric CO<sub>2</sub> and CH<sub>4</sub> mole fractions obtained with Picarro analyzers for sensitivity of cavity pressure to water vapor, *Atmos. Meas. Tech.*, 12, 1013–1027, <https://doi.org/10.5194/amt-12-1013-2019>, 2019.
- Rodríguez, S., González, Y., Cuevas, E., Ramos, R., Romero, P. M., Abreu-Afonso, J., and Redondas, A.: Atmospheric nanoparticle observations in the low free troposphere during upward orographic flows at Izaña Mountain Observatory, *Atmos. Chem. Phys.*, 9, 6319–6335, <https://doi.org/10.5194/acp-9-6319-2009>, 2009.
- Tsililingiris, P. T.: Thermophysical and transport properties of humid air at temperature range between 0 and 100 °C, *Energ. Convers. Manage.*, 49, 1098–1110, 2008.
- Van den Bosch, C. J. H. and Duijm, N. J.: Outflow and spray release, chap. 2, in: *Methods for the calculation of physical effects due to releases of hazardous substances (liquids and gases)*, 3rd edn., edited by: Van den Bosch, C. J. H. and Weterings, R. A. P. M., Organization of Applied Scientific Research, The Hague, the Netherlands, 2.1–2.179, 2005.
- WMO: Expert group recommendations, 18th WMO/IAEA Meeting on Carbon Dioxide, Other Greenhouse Gases and Related Tracers Measurement Techniques (GGMT-2015), La Jolla, CA, USA, 13–17 September 2015, GAW Report No. 229, World Meteorological Organization, Geneva, Switzerland, 1–51, 2016.
- Yver Kwok, C., Laurent, O., Guemri, A., Philippon, C., Wastine, B., Rella, C. W., Vuillemin, C., Truong, F., Delmotte, M., Kazan, V., Darding, M., Lebègue, B., Kaiser, C., Xueref-Rémy, I., and Ramonet, M.: Comprehensive laboratory and field testing of cavity ring-down spectroscopy analyzers measuring H<sub>2</sub>O, CO<sub>2</sub>, CH<sub>4</sub> and CO, *Atmos. Meas. Tech.*, 8, 3867–3892, <https://doi.org/10.5194/amt-8-3867-2015>, 2015.
- Zellweger, C., Steinbacher, M., and Buchmann, B.: Evaluation of new laser spectrometer techniques for in-situ carbon monoxide measurements, *Atmos. Meas. Tech.*, 5, 2555–2567, <https://doi.org/10.5194/amt-5-2555-2012>, 2012.
- Zellweger, C., Emmenegger, L., Firdaus, M., Hatakka, J., Heimann, M., Kozlova, E., Spain, T. G., Steinbacher, M., van der Schoot, M. V., and Buchmann, B.: Assessment of recent advances in measurement techniques for atmospheric carbon dioxide and methane observations, *Atmos. Meas. Tech.*, 9, 4737–4757, <https://doi.org/10.5194/amt-9-4737-2016>, 2016.